



## RESEARCH ARTICLE

# Novel method for collecting hippocampal interstitial fluid extracellular vesicles (EV<sup>ISF</sup>) reveals sex-dependent changes in microglial EV proteome in response to A $\beta$ pathology

Morgan C. Pait<sup>1</sup> | Sarah D. Kaye<sup>1</sup> | Yixin Su<sup>2</sup> | Ashish Kumar<sup>2</sup> | Sangeeta Singh<sup>2</sup> | Stephen C. Gironda<sup>1</sup> | Samantha Vincent<sup>1</sup> | Maria Anwar<sup>1</sup> | Caitlin M. Carroll<sup>1</sup> | James Andy Snipes<sup>1</sup> | Jingyun Lee<sup>3,4</sup> | Cristina M. Furdai<sup>3,4,5</sup> | Gagan Deep<sup>2,5,6,7</sup>  | Shannon L. Macauley<sup>1,7,8,9,10,11,12</sup> 

<sup>1</sup>Department of Physiology & Pharmacology, Wake Forest School of Medicine, Winston-Salem, North Carolina, USA

<sup>2</sup>Department of Cancer Biology, Wake Forest School of Medicine, Winston-Salem, North Carolina, USA

<sup>3</sup>Department of Internal Medicine, Section on Molecular Medicine, Wake Forest School of Medicine, Winston-Salem, North Carolina, USA

<sup>4</sup>Proteomics and Metabolomics Shared Resource, Wake Forest School of Medicine, Winston-Salem, North Carolina, USA

<sup>5</sup>Atrium Health Wake Forest Baptist Comprehensive Cancer Center, Wake Forest School of Medicine, Winston-Salem, North Carolina, USA

<sup>6</sup>Center for Research on Substance Use and Addiction, Wake Forest School of Medicine, Winston-Salem, North Carolina, USA

<sup>7</sup>J Paul Sticht Center for Healthy Aging and Alzheimer's Prevention, Wake Forest School of Medicine, Winston-Salem, North Carolina, USA

<sup>8</sup>Internal Medicine, Wake Forest School of Medicine, Winston-Salem, North Carolina, USA

<sup>9</sup>Alzheimer's Disease Research Center, Wake Forest School of Medicine, Winston-Salem, North Carolina, USA

<sup>10</sup>Center for Diabetes and Metabolism, Wake Forest School of Medicine, Winston-Salem, North Carolina, USA

<sup>11</sup>Cardiovascular Sciences Center, Wake Forest School of Medicine, Winston-Salem, North Carolina, USA

<sup>12</sup>Department of Physiology, University of Kentucky, Lexington, Kentucky, USA

## Correspondence

Shannon Macauley, Department of Physiology, University of Kentucky, 760 Press Avenue, Lexington, KY, 40508, USA. Email: [shannon.macauley@uky.edu](mailto:shannon.macauley@uky.edu)

Gagan Deep, Department of Cancer Biology, Wake Forest School of Medicine, Medical Center Boulevard, Hanes 5048, Winston-Salem, NC 27157, USA. Email: [gdeep@wakehealth.edu](mailto:gdeep@wakehealth.edu)

## Funding information

Averill Foundation; National Institutes of Health, Grant/Award Numbers: F31AG071119, K01AG050719, P30AG072947, P30CA012197, R01AG061805, R01AG068330, F31AG066302, F31AA030928; BrightFocus Foundation, Grant/Award Number: A20201775S

## Abstract

Brain-derived extracellular vesicles (EVs) play an active role in Alzheimer's disease (AD), relaying important physiological information about their host tissues. The internal cargo of EVs is protected from degradation, making EVs attractive AD biomarkers. However, it is unclear how circulating EVs relate to EVs isolated from disease-vulnerable brain regions. We developed a novel method for collecting EVs from the hippocampal interstitial fluid (ISF) of live mice. EVs (EV<sup>ISF</sup>) were isolated via ultracentrifugation and characterized by nanoparticle tracking analysis, immunogold labelling, and flow cytometry. Mass spectrometry and proteomic analyses were performed on EV<sup>ISF</sup> cargo. EV<sup>ISF</sup> were 40–150 nm in size and expressed CD63, CD9, and CD81. Using a model of cerebral amyloidosis (e.g., *APP<sup>swe</sup>*, *PSEN1dE9* mice), we found protein concentration increased but protein diversity decreased with A $\beta$  deposition. Genotype, age, and A $\beta$  deposition modulated proteostasis- and immunometabolic-related pathways. Changes in the microglial EV<sup>ISF</sup> proteome were sexually dimorphic and associated with a differential response of plaque associated microglia. We found that female APP/PS1 mice have more amyloid plaques, less

This is an open access article under the terms of the [Creative Commons Attribution-NonCommercial-NoDerivs](https://creativecommons.org/licenses/by-nc-nd/4.0/) License, which permits use and distribution in any medium, provided the original work is properly cited, the use is non-commercial and no modifications or adaptations are made.

© 2024 The Authors. *Journal of Extracellular Vesicles* published by Wiley Periodicals LLC on behalf of International Society for Extracellular Vesicles.

plaque associated microglia, and a less robust- and diverse- EV<sup>ISF</sup> microglial proteome. Thus, in vivo microdialysis is a novel technique for collecting EV<sup>ISF</sup> and offers a unique opportunity to explore the role of EVs in AD.

#### KEYWORDS

amyloid- $\beta$ , APP/PS1, exosomes, extracellular vesicles (EVs), interstitial fluid, microglia, plaques, sex differences

## 1 | INTRODUCTION

Brain-derived extracellular vesicles (EVs) can act as mediators and messengers of pathological conditions in Alzheimer's disease (AD) and other neurodegenerative disorders. Small EVs (sEVs) are present in nearly all tissues and biofluids, including the brain's interstitial fluid (ISF), cerebrospinal fluid (CSF), and blood. Exosomes are a subset of sEVs that are typically 40–150 nm in size (Jeppesen et al., 2019). They are endosomally derived and begin as intraluminal vesicles (ILVs) inside multivesicular bodies (MVBs) in the cell (Colombo et al., 2014, Console et al., 2019, Jeppesen et al., 2019). The MVBs can either fuse with lysosomes for degradation or with the plasma membrane to release ILVs into the extracellular space as exosomes (Colombo et al., 2014, Console et al., 2019, Jeppesen et al., 2019, Kolter & Sandhoff, 2005). The cargo found in exosomes and other sEVs is unique to their cell of origin and protected from degradation by a lipid bilayer as the vesicles move throughout the circulation (Cheng et al., 2014, Skotland et al., 2020). Their unique cargo of RNAs, proteins, and metabolites relays important physiological and metabolic information about the host cell or tissue in both homeostatic and pathological conditions. Since tissues like the brain are difficult to biopsy and brain-derived EVs can be detected in blood or CSF (Cha et al., 2019, Delgado-Peraza et al., 2021, Eren et al., 2022, Goetzl et al., 2015, Guo et al., 2020, Jia et al., 2019, Kumar et al., 2021, 2022), EVs are attractive biomarkers to facilitate the understanding, diagnosis, and staging of AD.

While EVs can carry proteins such as amyloid- $\beta$  (A $\beta$ ) and tau, the pathological hallmarks of AD, they can also relay information about the health and disease of the host cell or tissue based on their proteome, miRNAs, and metabolites (Lim et al., 2019, Ngolab et al., 2017, Rajendran et al., 2006, Sardar Sinha et al., 2018, Wang et al., 2017, Winston et al., 2019). Given this, uncovering how EVs are involved in AD pathogenesis is of great interest to the field. Currently, EVs are isolated from the blood, CSF, or postmortem brain tissue from AD human patients, mouse models of AD-like pathology, and nonhuman primates (Alvarez et al., 2022, Cha et al., 2019, Delgado-Peraza et al., 2021, Eren et al., 2022, Huang et al., 2020, Huang et al., 2022, Jia et al., 2019, Kumar et al., 2021, Lee et al., 2022, Longobardi et al., 2021, Longobardi et al., 2022, Muraoka et al., 2020, Muraoka et al., 2021, Muraoka et al., 2020, Polanco et al., 2016, Rather et al., 2022, Ruan et al., 2020, Spitzer et al., 2019, Utz et al., 2021, Winston et al., 2016, Winston et al., 2019, Yuyama et al., 2015). However, each compartment yields disparate results and has unique limitations. For example, neuronal-derived EVs in humans make up approximately 49% of brain tissue-EVs (Muraoka et al., 2020) but constitute only about 16% of CSF-EVs (Muraoka et al., 2020) and less than 15% of plasma-EVs (Kapogiannis et al., 2015). Microglia/macrophage-derived EVs make up only 4%–12% of CSF-EVs, which further differs from estimations in the blood (Guo et al., 2020). Similarly, miRNAs from brain- versus plasma-derived EVs from AD patients often fail to correlate with one another (Cheng et al., 2020). This suggests that compartments distal to the brain do not always reveal all disease-related or cell type-specific changes in brain EV populations, potentially biasing our understanding of disease progression. Brain-derived EVs isolated from CSF and blood also represent a heterogeneous pool of EVs and could fail to reveal brain region-specific changes associated with disease progression.

Over the past decade, advanced protocols for isolating sEVs from the extracellular space of postmortem brain tissue were developed to understand region-specific changes associated with pathology (Banigan et al., 2013, Cohn et al., 2021, Gallart-Palau et al., 2016, Huang et al., 2020, Hurwitz et al., 2018, Muraoka et al., 2020, Nguyen et al., 2022, Perez-Gonzalez et al., 2012, Pérez-González et al., 2017, Vella et al., 2017). Implementation of these methods demonstrated that levels of sEVs are differentially modulated by various AD risk factors (e.g., APOE4, Down syndrome, APP) as a function of age and disease severity (Gauthier et al., 2017, Hartley et al., 2015, Mathews & Levy, 2019, Peng et al., 2019, Perez-Gonzalez et al., 2012, Wisniewski et al., 1985). There are several limitations with this approach. First, EVs from postmortem brains may not fully reveal the active role EVs play in the AD cascade since they are sampled at one time-point, typically at an end stage of the disease, following a highly variable or lengthy postmortem interval. Thus, any dynamic changes in the in vivo brain could be lost with this approach. Some of these techniques use harsh methods of EV extraction, disrupting the brain cells which potentially leads to contamination of EVs with ILVs and other intracellular vesicles. Further, many of these studies are performed on whole brain, hemibrain, or pooled samples, losing the region-specific changes that occur in AD. Thus, despite these advances in brain EV isolation methods, the problem of collecting EVs from the extracellular space of an intact, in vivo brain, in a region-specific manner, persists. Therefore, developing new methods that detect dynamic changes in the EV pool in the brain's ISF in live animal models of AD is imperative.

Isolating EVs from the live brain can help us elucidate the role EVs play in AD as well as identify novel biomarkers of AD pathogenesis. Thus, we developed a novel method for collecting EVs from the hippocampal ISF of unanesthetized, freely moving

mice using in vivo microdialysis. To date, in vivo microdialysis is widely utilized in animal models of AD-like pathology for collecting A $\beta$ , tau, and other proteins and metabolites but heretofore untested as a method for collecting EVs from the ISF (Bero et al., 2011, Cirrito et al., 2008, Cirrito et al., 2003, Cirrito et al., 2005, Day et al., 2022, Holth et al., 2019, Macauley et al., 2015, Macauley et al., 2021, Stanley et al., 2016). By coupling in vivo microdialysis and EV isolation with proteomic profiling and bioinformatics, we hypothesized that this approach would allow us to characterize brain region- and cell type-specific changes in EVs relative to Alzheimer's-like pathology in vivo. In this study, we examined how the hippocampal ISF population of sEVs changes in a mouse model of Alzheimer's-related pathology, APPswe, PSEN1dE9 (APP/PS1) mice.

We found that in vivo microdialysis successfully captures small EVs from the hippocampal ISF (EV<sup>ISF</sup>) of live mice. Ultracentrifugation (UC), ExoQuick, and Size Exclusion Chromatography (SEC) could all successfully isolate EV<sup>ISF</sup>. Interestingly, age, sex, and amyloid pathology modulated EV<sup>ISF</sup> characteristics, specifically EV<sup>ISF</sup> number. Proteomic and bioinformatic analysis of EV<sup>ISF</sup> revealed that this method of EV collection selects for a unique EV population disparate from other studies. Surprisingly, EV<sup>ISF</sup> protein concentration increased while protein diversity within the EV<sup>ISF</sup> decreased with A $\beta$  pathology. EV<sup>ISF</sup> also revealed changes in proteostasis and neuroinflammation at 3-months in APP/PS1 versus WT mice, before amyloid plaques develop. A $\beta$  deposition further perturbed proteostasis and inflammation-related contents of EV<sup>ISF</sup>. Age, A $\beta$  deposition, and sex differentially modulated the EV<sup>ISF</sup> proteome based on the cell type of origin. Specifically, microglia-derived proteins correlated with ISF A $\beta$ , A $\beta$  deposition, and markers of microglial activation, but only in EV<sup>ISF</sup> of male APP/PS1 mice. We also observed sex dependent changes in plaque associated microglia that could be related to changes in the EV<sup>ISF</sup> microglial proteome. Thus, this study demonstrates for the first time that not only can EV<sup>ISF</sup> be collected from an in vivo brain using microdialysis, but this population of EVs is modulated by genotype, age, and A $\beta$  pathogenesis. Finally, EV<sup>ISF</sup> can detect sex-dependent changes in microglia-related EV proteins that correlate with AD-related pathology.

## 2 | METHODS

### 2.1 | Animals

3- and 9-month-old male ( $n = 46$ ) and female ( $n = 19$ ) mice heterozygous for the APPswe, PSEN1dE9 mutation (Jankowsky et al., 2004) (APP/PS1) or littermate controls (WT) on a B6C3 background were used in this study. Mice were given food and water ad libitum and maintained on a 12:12 light/dark cycle (Bateman et al., 2007, Kang et al., 2009, Roh et al., 2012). All protocols were approved by the Institutional Animal Care and Use Committee at Wake Forest School of Medicine.

### 2.2 | Workflow of EV<sup>ISF</sup> collection, isolation, and analysis

Hippocampal ISF was collected from 3- and 9-month-old APP/PS1 and WT mice using in vivo 1000 kDa microdialysis. Artificial cerebrospinal fluid (aCSF) was infused at 1.2  $\mu$ L/min with a syringe pump. ISF dialysate was collected via a peristaltic pump at 1  $\mu$ L/min into a 4°C refrigerated fraction collector. ExoQuick, Size Exclusion Chromatography (SEC), and Ultracentrifugation (UC) were tested in order to determine the preferred method of EV<sup>ISF</sup> isolation. Ultimately, EV<sup>ISF</sup> were isolated via UC and characterized by nanoparticle tracking analysis (NTA), transmission electron microscopy (TEM), and flow cytometry. Liquid chromatography-mass spectrometry/mass spectrometry (LC-MS/MS) was performed on the EV<sup>ISF</sup> protein cargo. Proteomic analyses were carried out by utilizing the Ingenuity Pathway Analysis (IPA), Database for Annotation, Visualization and Integrated Discovery (DAVID), and Search Tool for the Retrieval of Interacting Genes/Proteins (STRING) databases. The cell type sources of EV<sup>ISF</sup> proteins were determined using the publicly available brainrnaseq.org database (Zhang et al., 2014). The percentages of cell type-related proteins in EV<sup>ISF</sup> were revealed. Additionally, postmortem analyses were performed on the ISF and brain tissue via enzyme-linked immunosorbent assays (ELISAs) and immunohistochemistry (IHC), respectively (Figure 1).

### 2.3 | In vivo 1000 kDa microdialysis

In vivo 1000 kDa microdialysis was performed on a separate cohort of 3-month WT males ( $n = 21$ ) for EV isolation methods and another cohort of 3- and 9-month-old APP/PS1 and WT mice ( $n = 4-6$  mice/sex/age/group) for EV characterization and LC-MS/MS of EV<sup>ISF</sup>. A modified version of previously published methods for in vivo microdialysis was used (Holth et al., 2019, Roh et al., 2012, Yamada, 2018, Yamada et al., 2014, Yamada et al., 2011). A guide cannula (AtmosLM PEG-12, Amuza, Eicom) was stereotactically implanted into the left hippocampus (from bregma, A/P:  $-3.1$  mm, M/L:  $-2.5$  mm, D/V:  $-1.2$  mm at 12° angle) and secured into place with dental cement. Mice were transferred to Rattun recording chambers (BASi) then allowed to recover for  $\sim 72$  h. After the recovery period, a microdialysis probe (1000 kDa probe: 1000 kDa cut off, AtmosLM PEP-12-02, Amuza, Eicom) was inserted into the guide cannula. 0.15% bovine serum albumin (BSA, Sigma) in aCSF (1.3 mM CaCl<sub>2</sub>, 1.2 mM MgSO<sub>4</sub>, 3 mM

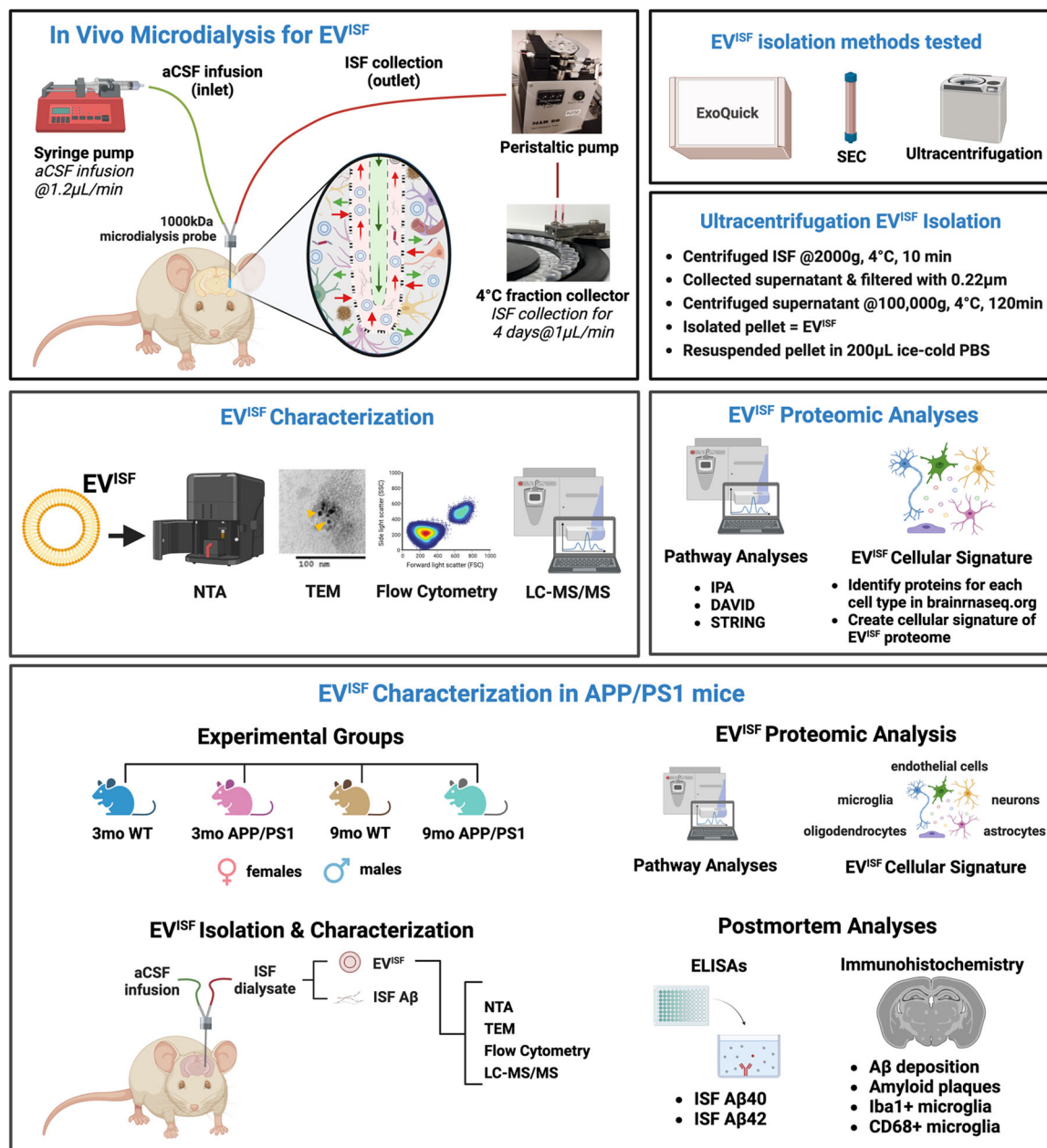


**FIGURE 1** Technical development of hippocampal interstitial fluid (ISF) extracellular vesicles (EV<sup>ISF</sup>) isolation, characterization, and analysis. Workflow of collection, isolation, characterization, and proteomic analysis of EV<sup>ISF</sup>. (*In Vivo Microdialysis for EV<sup>ISF</sup>*) ISF was collected from the hippocampus via in vivo microdialysis with a 1000 kDa pore-size probe. A schematic of the microdialysis including aCSF infusion (green arrows) and ISF collection (red arrows) is included. (*EV<sup>ISF</sup> isolation methods tested*) Three different methods for EV isolation (ExoQuick, Size-Exclusion Chromatography, and Ultracentrifugation) were tested on ISF. (*Ultracentrifugation EV<sup>ISF</sup> isolation*) Steps for isolating EVs from the ISF using ultracentrifugation. (*EV<sup>ISF</sup> Characterization*) EVs were characterized by nanoparticle tracking analysis (NTA), transmission electron microscopy (TEM), flow cytometry, and LC-MS/MS. (*EV<sup>ISF</sup> Proteomic Analyses*) Pathway analyses (IPA, DAVID, and STRING) were performed on the EV<sup>ISF</sup>. The EV<sup>ISF</sup> cellular signature was determined via utilization of the brainrnaseq.org database (49) to identify the cell-type origins of the EV<sup>ISF</sup> proteins. (*EV<sup>ISF</sup> Characterization in APP/PS1 mice*) EV<sup>ISF</sup> from the hippocampus of 3-month and 9-month WT and APP/PS1 mice, both sexes, were isolated and characterized. Proteomic analyses were performed on the EV<sup>ISF</sup>. Finally, postmortem analyses were performed on the collected ISF and brain tissue.

KCl, 0.4 mM KH<sub>2</sub>PO<sub>4</sub>, 25 mM NaHCO<sub>3</sub> and 122 mM NaCl; pH = 7.35) was filtered with a 0.10 μm membrane and infused using a syringe pump (KD Scientific) at a flowrate of 1.2 μL/min. ISF was collected at a flowrate of 1 μL/min via push-pull method with a peristaltic pump (MAB 20, SciPro). Samples were collected every 90 min into polypropylene tubes in a refrigerated fraction collector (MAB 85, SciPro) for ~72 h. Fractions were pooled, excluding first 6 h of acclimation, into 15 mL polypropylene tubes yielding a total volume of ~4 mL. Pooled samples were stored at -80°C as no difference was determined between analysis of EVs isolated from fresh versus frozen ISF. Following in vivo microdialysis, mice were euthanized via transcardial perfusion



with cold dPBS (Gibco Life Technologies Corporation, NY) with 0.3% heparin. The brain was bisected for biochemical and immunohistochemical analyses.

## 2.4 | Total EV isolation

Total EVs (TE) were isolated from ISF samples using three methods: (1) Ultracentrifugation (UC): ISF was harvested and centrifuged at 2000 g at 4°C for 10 min to remove cell debris. The supernatant was collected and filtered through 0.22 µm filters to remove large sized vesicles and further centrifuged (Beckman Coulter Optima Ultracentrifuge, Beckman Coulter, Brea, CA) at 100,000 g at 4°C for 120 min with a Type 70 Ti rotor to pellet sEVs. The supernatant was carefully removed, and sEV-containing pellets were resuspended in 200 µL of ice-cold PBS. (2) EVs protein concentration was evaluated by measuring absorbance at 280 nm using Nanodrop (Thermo Scientific, Waltham, MA). ExoQuick precipitation: ISF samples were centrifuged at 3000 × g for 15 min to remove cells and cell debris. The supernatant was collected in a sterile tube, and an appropriate volume of ExoQuick-TC was added, mixed, and incubated overnight at 4°C before centrifugation at 1500 × g for 30 min. The supernatant was collected and discarded, and the pellet was resuspended in sterile 1X PBS. (3) Size exclusion chromatography (SEC): EVs were isolated from ISF using Sephadex-G25 (GE Healthcare; Uppsala, Sweden) following the vendor's instruction. The column was washed with PBS (pH 7.4, 0.22 µm filtered). Subsequently, the column was equilibrated with 25 mL PBS and sample was added to enter the gel bed completely. The purified sample was eluted with an appropriate volume of PBS. The eluate was collected in 10 sequential fractions of 1 mL and each fraction was analysed for particle concentration (number/mL) by NTA as described below. Protein concentration of EVs was measured by a NanoDrop.

## 2.5 | Nanoparticle tracking analyses (NTA)

Quantification of the hydrodynamic diameter distribution and concentration (particle number/mL) of EVs was performed using the Nanosight NS300 (Malvern Instruments, UK) equipped with a violet laser (405 nm) and running software version NTA3.4. The instrument was primed using phosphate-buffered saline (PBS), pH 7.4, the temperature was maintained at 25°C, and calibrated using 100 and 200 nm polystyrene beads (Malvern Instruments, UK). EVs were diluted in 0.1 micron filtered DPBS and samples were injected in to flow cell at a flow rate of 0.05 ml/sec through an automated syringe pump. Five measurements (30 seconds each) were obtained for each sample and the average was plotted as representation of size distribution and concentration (particles/ml).

## 2.6 | Flow cytometry

Flow cytometry analysis was performed to evaluate the percentage of typical EV tetraspanin markers following methods and controls reported recently (Kumar et al., 2022, 2023; Mishra et al., 2023). TE were labelled with membrane labelling dye CellBrite 488 (Cat No: 30106; Biotium, California, USA) with and without the CD63-APC (Cat No: 143905, BioLegend, CA, USA) and CD81-PE (Cat No:104906, BioLegend, CA, USA) antibodies. EVs without dye were used as control to set the gate for positively labelled EVs. EVs labelled with dye but without CD63-APC/ CD81-PE antibody were used to set the gate for APC/ PE positive events. CD63-APC/ CD81-PE antibody and dye at the same dilution in PBS or aCSF (filtered through 0.22-micron filter) were also analysed. All samples were acquired on CytoFlex (Beckman Coulter Life Science, Indianapolis, United States) for 60 seconds at a low flow rate. Filtered PBS was run for 60 seconds in between the samples. Following sample acquisition, EVs were lysed by adding 0.25% triton-100 and acquired again to confirm the captured events were EVs. All the relevant controls used for flow cytometry analysis are presented in Figure S1.

## 2.7 | Immunogold labelling

EVs were fixed with 2% paraformaldehyde in PBS buffer (pH 7.4), then adsorbed for 1 hour to a carbon-coated grid. EVs were incubated with CD63 (Abcam, Cat. No. ab217345) or CD9 (Thermo Fisher, Cat. No. MA5-31980) primary antibody. A secondary antibody tagged with 10 nm gold particles was used. EVs were contrasted in 1% uranyl acetate for 5 min, and images were captured on Tecnai T12 transmission electron microscope. Samples treated with only gold-labelled secondary antibody were used as a negative control.

## 2.8 | EV<sup>ISF</sup> proteomic profiling via LC-MS/MS

EV<sup>ISF</sup> were isolated from ISF by ultracentrifugation as described above. Proteomic profiling was performed on EV<sup>ISF</sup> from 37 individual mice: 3-month WT ( $n = 8$ ), 3-month APP/PS1 ( $n = 8$ ), 9-month WT ( $n = 10$ ), and 9-month APP/PS1 ( $n = 10$ ). With our approach, LC-MS/MS was performed on EV<sup>ISF</sup> from each individual mouse (i.e., samples were not pooled). EV<sup>ISF</sup> were briefly treated with trypsin at 1:100 (enzyme:EV<sup>ISF</sup> protein) ratio for 2 h at 37°C to remove proteins, and shaved EVs were pelleted again by ultracentrifugation at 200,000  $\times$  g for 3 h. Core proteins were prepared for LC-MS/MS analysis according to the method reported by us recently (Kumar et al., 2021, Rather et al., 2022). Samples were analysed on a LC-MS/MS system consisting of an Orbitrap Velos Pro Mass Spectrometer (Thermo Scientific, Waltham, MA) and a Dionex Ultimate3000 nano-UPLC system (Thermo Scientific, Waltham, MA). An Acclaim PepMap 100 (C18, 5  $\mu$ m, 100 Å, 100  $\mu$ m  $\times$  2 cm) trap column and an Acclaim PepMap RSLC (C18, 2  $\mu$ m, 100 Å, 75  $\mu$ m  $\times$  50 cm) analytical column were employed for peptide separation. MS spectra were acquired by data-dependent scans, and then searched using Sequest HT within the Proteome Discoverer v2.2 (Thermo Scientific, Waltham, MA) and UniProt human protein FASTA database (20,258 annotated entries, Feb 2018). Search parameters were as follows: FT-trap instrument, parent mass error tolerance of 10 ppm, fragment mass error tolerance of 0.6 Da (monoisotopic), variable modifications of 16 Da (oxidation) on methionine. Fixed modification of 57 Da (carbamidomethylation) was applied to cysteine for core protein identification.

## 2.9 | Determination of cell type-related proteins in EV<sup>ISF</sup>

The gene names of EV<sup>ISF</sup> proteins were determined using UniProt.org (UniProt Consortium 2021). Brainrnaseq.org database (Zhang et al., 2014) determined cell type origin(s) (microglia, neuron, oligodendrocyte, astrocyte, endothelial cell) of EV<sup>ISF</sup> proteins. If a protein was represented in more than one cell type, it was counted for each cell type it was found in. Therefore, a specific protein was considered part of a particular cell type (e.g., microglia) even if it was also found in another (e.g., astrocytes). A protein was considered present in a particular cell type if its presence in that cell type crossed the half-way point of the highest FPKM point on the y-axis. Within each animal, the total number of times a particular cell type was identified was summed. A percentage was determined by dividing that summed number by the sum total of all cell types found in that animal and multiplying by 100. Significant effects were determined using one-way ANOVAs with Tukey's multiple comparisons posthoc tests.

## 2.10 | Immunohistochemistry and quantification for A $\beta$ and CD68 staining

3-month and 9-month WT and APP/PS1 mice were anesthetized with isoflurane and transcardially perfused with cold DPBS with 0.3% heparin. The brains were removed and fixed in 4% paraformaldehyde for at least 48 h at 4°C. Prior to sectioning, the brains were cryoprotected in 30% sucrose then sectioned on a freezing microtome at 50  $\mu$ m. Three serial sections (300  $\mu$ m apart) through the anterior-posterior aspect of the hippocampus were immunostained for either A $\beta$  deposition or CD68. A $\beta$  deposition. Free-floating sections were stained for A $\beta$  deposition using a biotinylated, HJ3.4 antibody (anti-A $\beta$ <sub>1-13</sub>, mouse monoclonal antibody, a generous gift from the Holtzman Lab, Washington University). CD68 staining. Free floating sections were blocked with 3% donkey serum and incubated overnight with rat anti-CD68 (1:200, Bio-Rad, MC A1957). A $\beta$  deposition and CD68 staining were both developed with a Vectastain ABC kit and DAB reaction. The brain sections were imaged with the Wake Forest Imaging Core NanoZoomer slide scanner and quantified as described previously (Bero et al., 2011, Roh et al., 2012). Data is represented as area fraction means  $\pm$  standard error of the mean (SEM). Mean reactivity and percent area occupied by HJ3.4 or CD68 were quantified with ImageJ software (National Institutes of Health) by a blinded researcher as previously described (Bero et al., 2011, Roh et al., 2012). Statistical significance was determined using a one-way ANOVA with multiple comparisons Tukey's tests.

## 2.11 | Immunohistochemistry and quantification for X34, IBA1, and CD68 staining

Three 50  $\mu$ m brain sections of the anterior cortex were taken from 3-month-old and 9-month-old WT and APP/PS1 mice. Free-floating sections were incubated in X34 (Sigma) for 20 min at room temperature in a 60% PBS/40% EtOH mix. Sections were washed briefly three times with 60% PBS/40% EtOH and then two times in PBS before blocking. Following blocking, sections were incubated in IBA1 (Wako 019-1941; antirabbit 1:1000; 019-1941) and CD68 (Abcam ab201340; antimouse 1:150) and kept at 4°C overnight with slow agitation. The following morning, sections were washed with PBS and then blocked and incubated with corresponding secondaries for 2 h at room temperature. The secondary for IBA1 was goat- antirabbit Alexa fluorophore 488 (Invitrogen/Thermo Fisher) while the secondary for CD68 was goat- antimouse Alexa fluorophore 594 (Invitrogen/Thermo

Fisher). After the 2 h incubation, sections were briefly washed in PBS again and mounted with fluoromount and coverslipped. Sections were imaged using a Nikon Ci laboratory microscope. For all analyses, images were acquired using a 20x objective with  $2880 \times 2048$  pixel resolution. For quantification of plaques, microglia, and CD68, images were imported to Fiji and thresholding methods were performed for each individual channel. After thresholding, the area fraction was identified for each channel and each image. Mixed-effects analyses were performed and followed by Tukey's post hoc tests to identify group differences. In addition to area fraction measurements, all three channels for each image were merged to perform colocalization analyses using EzColocalization (Stauffer et al., 2018). A threshold overlap score (TOS), a measure of colocalization, was determined for each image and compiled for each group. Differences in TOS between the groups were assessed using a mixed-effects analysis and Tukey's posthoc analyses.

## 2.12 | A $\beta$ 40 and A $\beta$ 42 ELISAs

Hippocampal ISF samples from 3-month and 9-month APP/PS1 mice and WT mice ( $n = 4-6$ /group) collected from microdialysis experiments were analysed for A $\beta$ 40 and A $\beta$ 42 using sandwich ELISAs as previously described (Bero et al., 2011, Cirrito et al., 2003, Cirrito et al., 2005, Macauley et al., 2015). Briefly, A $\beta$ 40 & A $\beta$ 42 were quantified using monoclonal capture antibodies (generous gifts from Dr. David Holtzman, Washington University) targeted against amino acids 33-40 (HJ2) or 35-42 (HJ7.4) respectively. For detection, a biotinylated monoclonal antibody against the central domain amino acids 13-28 (HJ5.1B) was used, followed by streptavidin-poly-HRP-40 (Fitzgerald). The assay was developed using Super Slow TMB (Sigma) and the plates were read on a Bio-Tek Synergy H1 plate reader at 650 nm. Standard curves with known A $\beta$  standards related optical density measures to A $\beta$  concentrations. Statistical significance was determined using a one-way ANOVA. Data is represented by means  $\pm$  SEM.

## 2.13 | Data analysis: IPA analysis

The proteomics data was analysed using IPA (QIAGEN Inc.) as previously described (64-66). Briefly, identified proteins were functionally assigned to canonical pathways and subsequently mapped to the most significant networks generated from previous publications and public protein interaction databases. Canonical pathways were presented as  $-\log_{10}(p\text{-value})$ . DAVID analysis: DAVID Bioinformatics Resources 6.8 was utilized for Gene Ontology (GO) analysis of hippocampal EV<sup>ISF</sup> proteins. GO terms for the top "Biological process," "Cellular component," "Molecular function," and "Tissue" were presented as  $-\log_{10}(\text{FDR } p\text{-value}) \geq 1.3$ . Kyoto Encyclopedia of Genes and Genomes (KEGG) pathways obtained via DAVID were also presented as  $-\log_{10}(\text{FDR } p\text{-value}) \geq 1.3$ . STRING analysis: STRING database (Szklarczyk et al., 2023) was utilized for determining the top 20 biological processes of EV<sup>ISF</sup> proteins. Correlation analyses: To define the relationships between all metrics measured, correlational analyses were performed between the following variables to determine the relationship: 1) ISF A $\beta$ 40, 2) ISF A $\beta$ 42, 3) A $\beta$  deposition, 4) CD68 staining and 5) EV<sup>ISF</sup> cell type % (neuronal, astrocyte, etc.). Correlation coefficients ( $r$ ), coefficients of determination ( $R^2$ ), and  $p$ -values ( $p$ ) were calculated for each relationship to define the strength of the interaction. Histological and biochemical analyses: IHC images were evaluated for percent area of A $\beta$ 40+ and CD68+ in the hippocampus and cortex using ImageJ (National Institute of Health) software and compared to WT. Additionally, all histological markers were compared between sexes to evaluate difference in AD-related burden. Significant effects were determined using one-way ANOVAs with posthoc tests. One-way ANOVAs or t-tests compared histochemical and biochemical readouts between groups. Statistical significance for all analyses was set at  $p < 0.05$ . Prism 9 (GraphPad Software, Inc., San Diego, CA) was used for statistical analyses. Venn diagram comparing the EV<sup>ISF</sup> proteins from the four mouse groups was created using R Studio R package version 1.7.1.R "VennDiagram: Generate High-Resolution Venn and Euler Plots" by Hanbo Chen (2021) <https://CRAN.R-project.org/package=VennDiagram>. Three-way comparison of the EV<sup>ISF</sup> proteins, Choi et al EV dataset (Choi et al., 2013), and ExoCarta Top 100 list (Keerthikumar et al., 2016) was generated via the Whitehead Institute for Biomedical Research Bioinformatics and Research Computing public tools website: [barc.wi.mit.edu/tools/compare\\_3\\_lists/](http://barc.wi.mit.edu/tools/compare_3_lists/). The three-way comparison of the EV<sup>ISF</sup> protein dataset to the human brain tissue-derived (Muraoka et al., 2020) and mouse brain tissue-derived (Muraoka et al., 2021) EV datasets was also generated via [barc.wi.mit.edu/tools/compare\\_3\\_lists/](http://barc.wi.mit.edu/tools/compare_3_lists/).

## 3 | RESULTS

### 3.1 | In vivo microdialysis as a novel method for collecting EV<sup>ISF</sup> from the hippocampus of live, freely moving, unanesthetized mice

Our preliminary studies demonstrated that the 1000kDa microdialysis probe was the best approach for isolating EV<sup>ISF</sup> from live, freely moving mice. Using coordinates from Paxinos and Franklin's mouse brain atlas (from bregma, A/P:  $-3.1$  mm, M/L:

−2.5 mm, D/V: −1.2 mm at 12° angle), a microdialysis guide cannula and 1000 kDa probe were stereotactically implanted into the mouse hippocampus and probe placement confirmed histologically postmortem (Figure 2a). The collection of brain region-specific ISF from the hippocampus via in vivo microdialysis is well-established (Bero et al., 2011, Cirrito et al., 2003, Grizzanti et al., 2023, Harris et al., 2016, Stanley et al., 2016) and we adapted this approach to isolate EV<sup>ISF</sup>. Our initial characterization of EV<sup>ISF</sup> used hippocampal ISF collected from 3-month-old WT and APP/PS1 mice, where sEVs were isolated via ultracentrifugation. The 1000 kDa probes successfully collected small EVs in the size range of 100–150 nm, with an average size of  $131.3 \pm 4.476$  nm (Théry et al., 2018) (Figure 2b). The average particle concentration was  $3.738 \times 10^7 \pm 1.225 \times 10^7$  particles/ml, with an average protein concentration of  $0.0883 \pm 0.0055$   $\mu\text{g}/\mu\text{l}$  in EV<sup>ISF</sup>. Immunogold labelling for CD63 and CD9 demonstrated that tetraspanin EV markers were present on the surface of the EV<sup>ISF</sup> (Figure 2c, additional full images presented in Figure S2a and S2b). Together, this demonstrated that we could collect sEVs using our in vivo microdialysis approach.

Next, we compared ultracentrifugation (UC) to ExoQuick and Size Exclusion Chromatography (SEC) to determine the optimal method for isolating EV<sup>ISF</sup>. NTA was used to characterize the mean size and concentration of EV<sup>ISF</sup> isolated for each method. When comparing EV size, ExoQuick isolated EV<sup>ISF</sup> with a larger size compared to both UC ( $p = 0.0001$ ) and SEC ( $p = 0.0031$ ; Figure 2d, left panel). There was no difference in the concentration of EV<sup>ISF</sup> across all three isolation methods (Figure 2d, right panel). The distribution for the various size ranges is shown in Figure 2 revealing that UC and SEC enriched for smaller particles (less than 200 nm), while a large percentage of bigger sized particles (more than 200 nm) were observed with ExoQuick (Figure 2e). EV<sup>ISF</sup> isolated via all three methods were analysed via flow cytometry to determine the percentage of CD63- and CD81-positive EV<sup>ISF</sup>, markers used to identify exosome-enriched sEVs. CD63-positive EV<sup>ISF</sup> were detected via UC, ExoQuick, and SEC isolation methods with no difference between groups (Figure 2f,g). However, SEC resulted in more CD81-positive EV<sup>ISF</sup> compared to UC ( $p = 0.0186$ ) but not ExoQuick (Figure 2f,g). Therefore, ExoQuick and SEC also supported the isolation of EVs from the ISF following in vivo microdialysis. However, given the higher particle number obtained by UC method, for all following experiments, EV<sup>ISF</sup> isolations were performed via ultracentrifugation. Since aCSF with 0.15% BSA was used for the microdialysis dialysate, we also measured the particle concentration in 0.15% BSA in aCSF in parallel. NTA showed that aCSF particle concentration was less than 1% compared to EV<sup>ISF</sup> isolated by UC method (Figure S3). This data rules out any major contribution to particle numbers by 0.15% BSA-aCSF aggregates.

### 3.2 | Age and A $\beta$ pathology differentially modulate EV<sup>ISF</sup> characteristics in APP/PS1 and WT mice

ISF was collected from 3- and 9-month-old WT and APP/PS1 mice for EV<sup>ISF</sup> isolation and characterization. In accordance with the literature, no A $\beta$  deposition was found in the hippocampus or cortex of APP/PS1 male and female mice at 3-months of age (Figure 3a,b) (Jankowsky et al., 2004). By 9-months, A $\beta$  deposition was present in both male and female APP/PS1 mice (Figure 3a,b). Female APP/PS1 mice had increased hippocampal A $\beta$  deposition ( $p = 0.0113$ ), while amyloid plaque burden was less in males of the same age (Figure 3b) (Jankowsky et al., 2004). In cortex, plaque pathology increased with age in both female ( $p < 0.0001$ ) and male APP/PS1 mice ( $p = 0.0026$ ), with amyloid plaque pathology more demonstrative in female than male mice (Figure 3b).

The ISF pool of A $\beta$  is highly dynamic and reflects acute changes in the production and clearance of A $\beta$ , leading to changes in A $\beta$  aggregation and amyloid plaque formation (Cirrito et al., 2003). A $\beta$  is aggregatory prone and a key component of amyloid plaques, a hallmark of AD pathology. A $\beta$ 42 is the more toxic and aggregatory prone, but less abundant form of A $\beta$  in the ISF and CSF. As A $\beta$  begins to aggregate, A $\beta$ 42 levels drop in the CSF because it is sequestered in amyloid plaques within the brain parenchyma. Therefore, we characterized how ISF A $\beta$  levels change as a function of pathology, age, and sex, as well as EV<sup>ISF</sup>, in APP/PS1 and WT mice. While several studies explored how ISF A $\beta$  levels changed relative to amyloid pathology, no study to date has investigated changes in specific ISF A $\beta$  species relative to age, genotype, and sex (Cirrito et al., 2003, Hong et al., 2011). Due to transgenic overexpression, ISF A $\beta$ 40 levels were greater in APP/PS1 mice compared to WT. This effect was lost in 9-month-old APP/PS1 males compared to age-matched WT, where ISF A $\beta$ 40 levels decreased in APP/PS1 males ( $p = 0.0449$ ). Interestingly, we did not observe the same reduction in ISF A $\beta$ 40 in 9-month-old females, suggesting a sexual dimorphic response to ISF A $\beta$ 40 proteostasis and amyloid plaque formation (Figure 3c). ISF A $\beta$ 42 levels increased in APP/PS1 mice compared to WT. ISF A $\beta$ 42 levels trended towards a decrease with plaque pathology in APP/PS1 for both males ( $p = 0.0808$ ) and females ( $p = 0.0522$ ) compared to age and sex-matched WT (Figure 3d). Together, these data demonstrate A $\beta$  species-, sex-, age-, and pathology-dependent changes in ISF A $\beta$  levels relative to A $\beta$  aggregation.

EV<sup>ISF</sup> from WT and APP/PS1 mice were characterized for size and concentration via NTA (Figure 3e,f). EV<sup>ISF</sup> concentration increased with age in the WT ( $p = 0.0098$ ) but not in the APP/PS1 mice (Figure 3e). Interestingly, 9-month APP/PS1 mice trended towards a decrease in EV<sup>ISF</sup> concentration compared to age-matched WT ( $p = 0.0592$ ; Figure 3e). When stratified by sex, EV<sup>ISF</sup> concentration increased with age in WT males ( $p = 0.0028$ ; Figure 3f). EV<sup>ISF</sup> concentration decreased in 9-month-old APP/PS1 males compared to age-, sex-matched WT mice ( $p = 0.0458$ ; Figure 3f). This suggests a potential sex-specific change in EV<sup>ISF</sup>



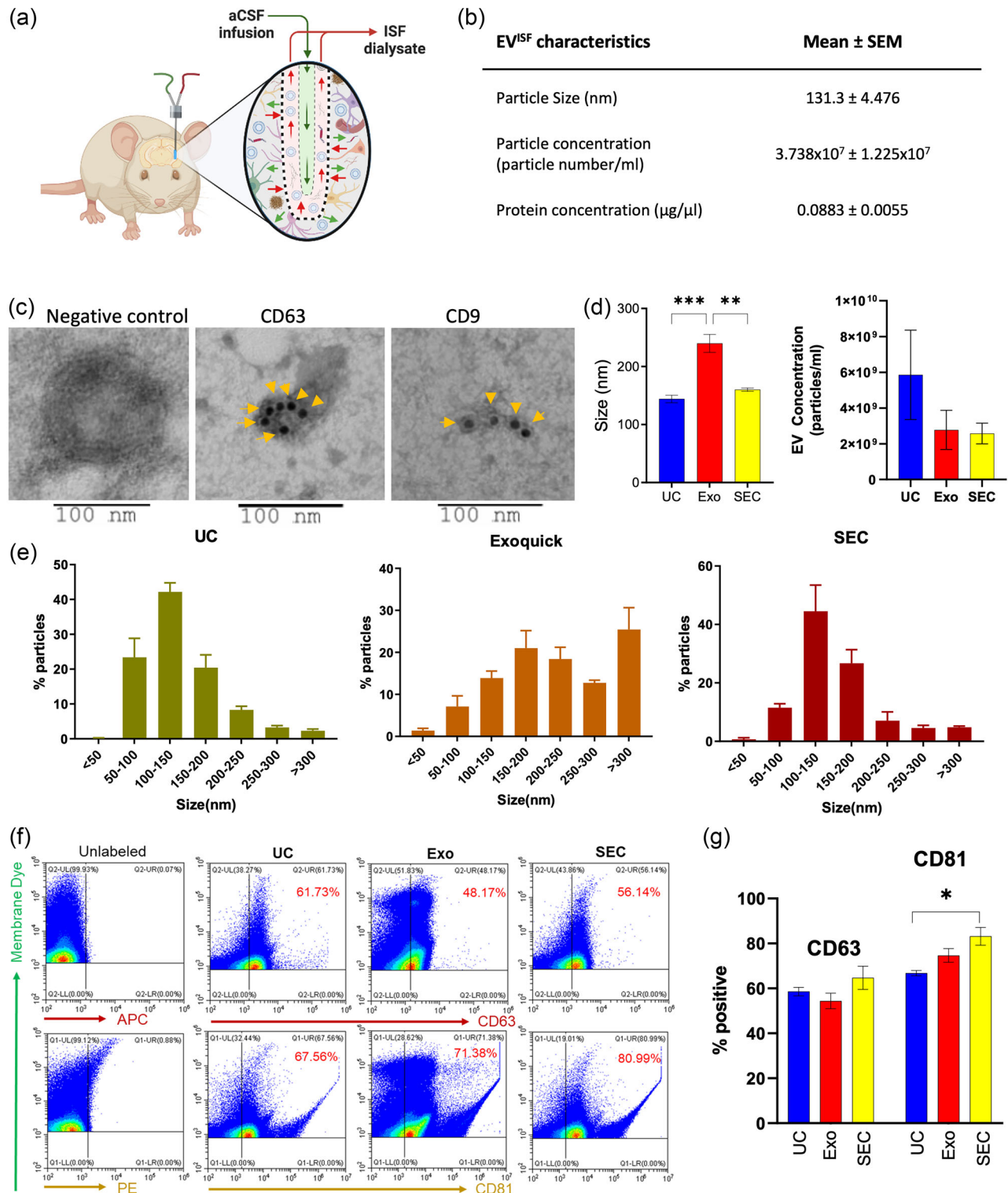


**FIGURE 2** In vivo microdialysis successfully collects hippocampal EV<sup>ISF</sup>, confirmed by multiple EV isolation methods. (a) Schematic of 1000 kDa in vivo microdialysis for EV<sup>ISF</sup> isolation. Artificial cerebrospinal fluid (aCSF) with .15% BSA (green arrows) is infused through the microdialysis probe and hippocampal interstitial fluid (ISF) is simultaneously collected (red arrows) using an infusion pump and push-pull pump, respectively. Metabolites, proteins, and EVs freely diffuse across the membrane and were collected for further analysis ex vivo. (b) Table containing initial EV<sup>ISF</sup> characterization. EV<sup>ISF</sup> particle size, particle concentration, and protein concentration were assessed. Protein concentrations were assessed after EV pellets were dissolved in PBS and the protein concentration of EVs was estimated by nanodrop. (c) Immuno-gold labelling was performed to confirm the presence of CD63 and CD9 on EV isolated by UC. Solid yellow arrows represent the presence of these markers on EVs surface. (d) EV<sup>ISF</sup> were isolated from ISF samples ( $n = 6$ ) using three different methods: UC, Exo = ExoQuick, and SEC = Size Exclusion Chromatography. Nanoparticle tracking analysis (NTA) was performed to estimate the mean size and concentration (particles/ml) of EV<sup>ISF</sup>, isolated using UC ( $n = 6$ ), Exo ( $n = 6$ ) and SEC ( $n = 3$ ) methods. Exo isolated larger EVs than both UC ( $p = 0.0001$ ) and SEC ( $p = 0.0031$ ). Graphs represent mean  $\pm$  SEM. (e) Size distribution of particles (%) was calculated from the nanoparticle analysis data and plotted for each isolation method. Bars represents size/ concentration  $\pm$  SEM. (f) Flow cytometry analysis was performed to analyse the CD63+ and CD81+ EVs

(Continues)

**FIGURE 2** (Continued)

percentage in EV<sup>ISF</sup> ( $n = 3$  each for method). EV<sup>ISF</sup> were labelled with membrane labelling dye (CellBrite 488) and followed by CD63 (APC) and CD81 (PE) tagged antibodies. Dye positive EVs (representing membrane bound particles) on Y-axis were gated and analysed for CD63/81 positive EVs. EV<sup>ISF</sup> without antibody was used to set the gate for APC/PE positive EVs. Right shift in the APC/PE fluorescence showed the positive EVs. (g) The CD63+ and CD81+ EVs in EV<sup>ISF</sup>, analysed by flow cytometry, isolated with different methods ( $n = 3$  each method) were plotted as mean  $\pm$  SEM. The % of CD63+ EVs was the same across isolation methods. SEC isolated a greater % of CD81+ EVs than UC ( $p = 0.0186$ ) but not Exo. Unpaired, two-tailed, Student's t-test:  $p < 0.05^*$ ,  $p < 0.01^{**}$ ,  $p < 0.001^{***}$ .  $N = 3$ –6 per group. One-way ANOVA, multiple comparisons Tukey's tests:  $p < 0.05^*$ ,  $p < 0.01^{**}$ ,  $p < 0.001^{***}$ .  $N = 5$ –16 per group, both sexes.

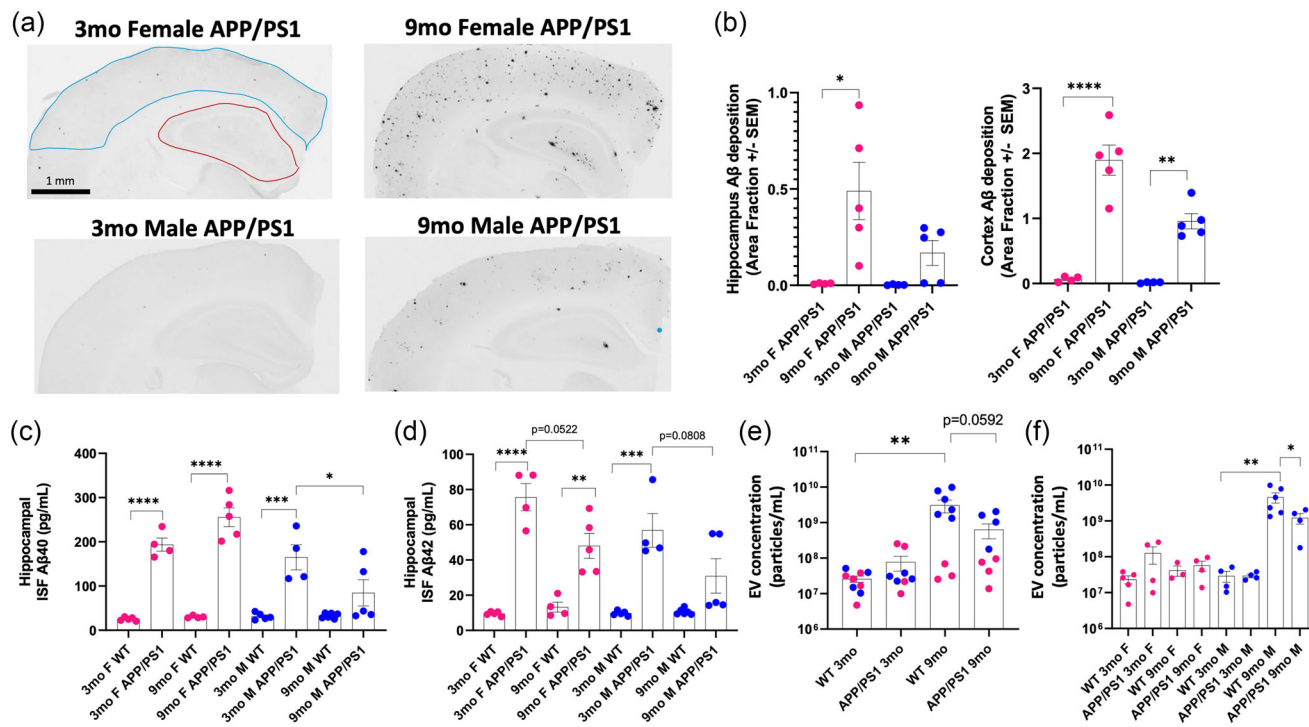


**FIGURE 3** Age and Aβ pathology related changes in ISF Aβ, Aβ deposition, and EV<sup>ISF</sup> characteristics in APP/PS1 and WT mice. (a) Representative images of Aβ deposition in 3-month and 9-month APP/PS1 mice, both sexes (red = hippocampus; blue = cortex). (b) Aβ deposition in hippocampus and cortex was quantified and presented as Area Fraction. Plaque burden in hippocampus increased with age in female APP/PS1 mice ( $p = 0.0113$ ) but not in males. In cortex of APP/PS1, Aβ deposition increased in both females ( $p < 0.0001$ ) and males ( $p = 0.0026$ ) with age. (c) ELISAs for Aβ40 were performed on hippocampal ISF samples. ISF Aβ40 levels were higher in APP/PS1 compared to WT (3 mo F WT vs. 3 mo F APP/PS1:  $p < 0.0001$ , 9 mo WT F vs. 9 mo F APP/PS1:  $p < 0.0001$ , 3 mo M WT vs. 3 mo M APP/PS1:  $p = 0.0001$ ) except for in 9-month WT vs. 9-month APP/PS1 males. ISF Aβ40 levels decreased in 9-month APP/PS1 males ( $p = 0.0449$ ) but not females. (d) ELISAs for Aβ42 were performed on hippocampal ISF samples. ISF Aβ42 levels were increased in APP/PS1 mice compared to WT (3 mo F WT vs. 3 mo F APP/PS1:  $p < 0.0001$ , 9 mo WT F vs. 9 mo F APP/PS1:  $p = 0.0066$ , 3 mo M WT vs. 3 mo M APP/PS1:  $p = 0.0001$ ) except for in 9-month WT vs. 9-month APP/PS1 males. ISF Aβ42 levels had a trending decrease with plaque pathology in APP/PS1 in both males ( $p = 0.0808$ ) and females ( $p = 0.0522$ ). (e) EV<sup>ISF</sup> concentration (particle number/mL) increased with age in WT mice ( $p = 0.0098$ ) but not APP/PS1. However, 9-month APP/PS1 EV<sup>ISF</sup> concentration had a trending decrease compared to 9-month WT ( $p = 0.0592$ ). (f) EV<sup>ISF</sup> concentration was separated by sex, age, and genotype. EV<sup>ISF</sup> concentration increased with age in WT male mice ( $p = 0.0028$ ). EV<sup>ISF</sup> concentration decreased with plaque pathology between 9-month WT and 9-month APP/PS1 males ( $p = 0.0458$ ) but not females. One-way ANOVA, multiple comparisons Tukey's tests:  $p < 0.05^*$ ,  $p < 0.01^{**}$ ,  $p < 0.001^{***}$ ,  $p < 0.0001^{****}$ . Scale bar = 250 μm.  $N = 3$ –6 per group.

uptake or release when amyloid plaques are present in APP/PS1 males (Figure 3f). EV<sup>ISF</sup> size was unchanged with genotype, age, or sex (data not shown).

### 3.3 | Proteomics of total hippocampal EV<sup>ISF</sup>

LC-MS/MS proteomic results from total hippocampal EV<sup>ISF</sup> revealed 436 proteins in EV<sup>ISF</sup> present in at least 2 or more mice (Table S1). DAVID analysis of all 436 proteins resulted in Gene Ontology (GO) terms for specific “Biological processes” which were grouped into related categories including proteostasis (32%), RNA processing (19%), immune function (10%), cell growth (6%), cellular trafficking (6%), glucose metabolism (6%), vascular health (6%), wound healing (4%), cellular excitability (3%), cellular structure (3%), apoptosis (2%), circadian rhythms (1%), DNA repair (1%), and lipid metabolism (1%) (Figure 4a). This confirms that the EV population isolated from the hippocampal ISF has shared characteristics of known EV functions and

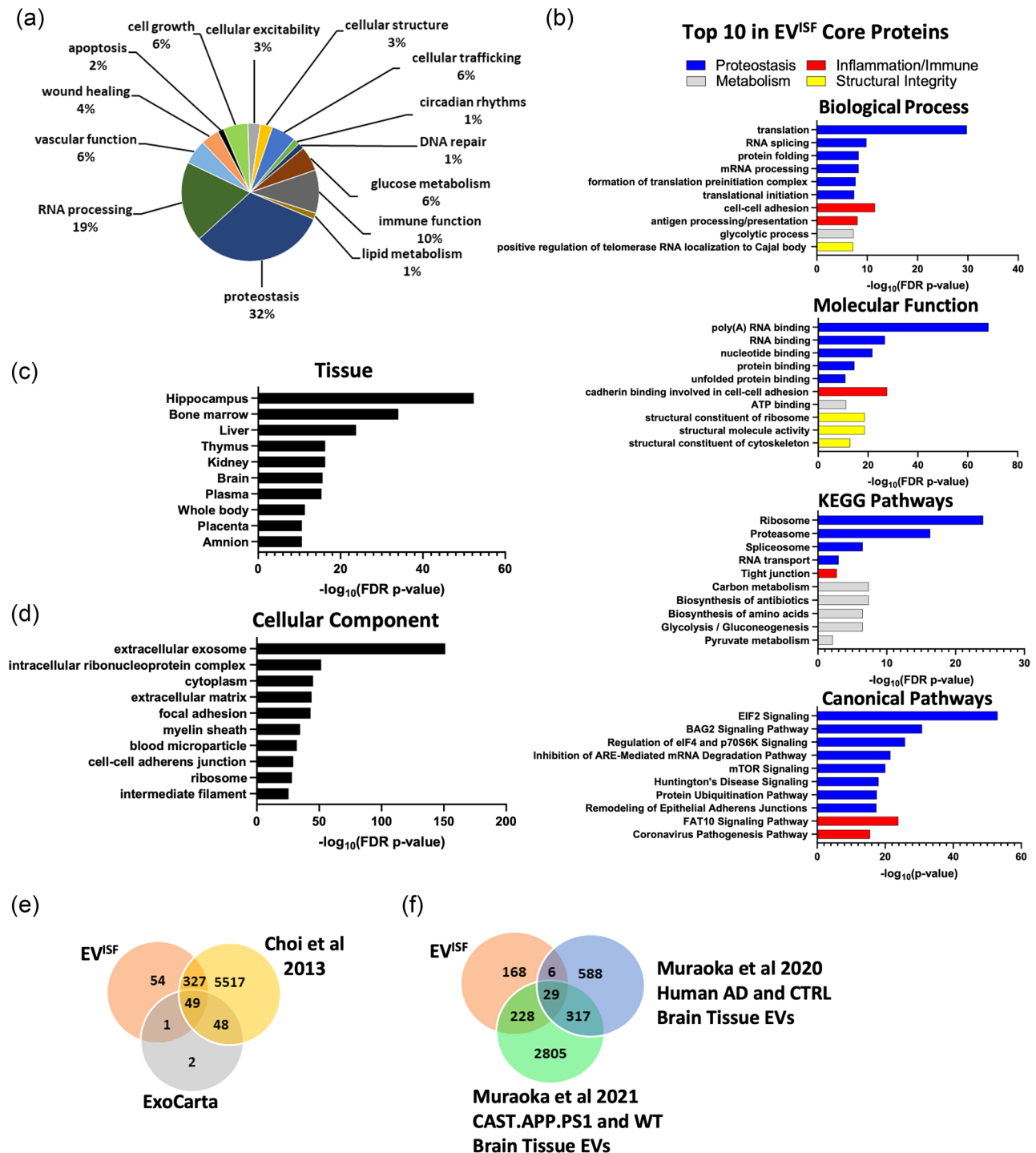


**FIGURE 4** EV<sup>ISF</sup> Proteomics: (a) Biological process groups for all EV<sup>ISF</sup> proteins. (b) Top 10 Biological Processes, Molecular Functions, KEGG Pathways, and IPA Canonical Pathways for all EV<sup>ISF</sup> proteins. Blue = Proteostasis, Red = Inflammation/Immune, Green = Metabolism, and Yellow = Structural Integrity. (c) DAVID analyses were performed on all the isolated EV<sup>ISF</sup>. The top UP\_Tissue result was Hippocampus. (d) The top GOTERM\_Cellular Component result was “extracellular exosome.” (e) Venn Diagram comparing EV proteins between the Choi et al 2013, ExoCarta Top 100, and EV<sup>ISF</sup> datasets. (f) Venn Diagram comparing EV proteins between the Muraoka et al 2020, Muraoka et al 2021, and EV<sup>ISF</sup> datasets.

relationships (Brás et al., 2022, Buzas, 2023, Datta Chaudhuri et al., 2020, Gallart-Palau et al., 2019, Kakarla et al., 2020, Meng et al., 2020, O’Brien et al., 2020, Oggero et al., 2019, Su et al., 2021, van Niel et al., 2018, Wei et al., 2020, Yeung et al., 2022). The top 10 GO terms for “Biological process,” “Molecular function,” KEGG pathways, and Canonical pathways were identified using DAVID and IPA analyses (Figure 4b). These top 10 results were clustered into categories related to proteostasis, inflammation/immune function, metabolism, and cellular structural integrity (Figure 4b). Further DAVID analysis of the EV<sup>ISF</sup> proteomic data confirmed hippocampus as the top GO term “Tissue,” validating the efficacy of this technique to detect EV<sup>ISF</sup> in a particular brain

region (Figure 4c). This was not surprising since our microdialysis probe was directly implanted into the ventral hippocampus. DAVID analysis also verified extracellular exosomes as the top GO term for “Cellular component” in the EV<sup>ISF</sup> dataset (Figure 4d). Comparison of the 436 proteins found in EV<sup>ISF</sup> to the Top 100 ExoCarta proteins list (Keerthikumar et al., 2016) and a proteomic EV dataset from Choi et al. (Choi et al., 2013) revealed 49 shared proteins among the three groups (Figure 4e). Interestingly, 54 proteins were unique to EV<sup>ISF</sup>. EV<sup>ISF</sup> also shared 29 proteins with EVs isolated from postmortem mouse brain tissue (Muraoka et al., 2021) and human brain tissue (Muraoka et al., 2020). This comparison revealed 168 proteins unique to hippocampal EV<sup>ISF</sup> (Figure 4f). Assessment of the unique EV<sup>ISF</sup> proteins from both Venn diagrams (Figure 4e,f) resulted in 45 proteins unique to EV<sup>ISF</sup> only (see Table S2). Thus, although hippocampal EV<sup>ISF</sup> collected via in vivo microdialysis shared cargo with EVs isolated with other techniques, they are a unique pool of EVs with distinctive cargo not typically present in other EV datasets.

### 3.4 | Age and A $\beta$ pathology differentially alter EV<sup>ISF</sup> protein concentration, protein diversity, and biological processes

EV<sup>ISF</sup> protein concentration increased with age in both WT ( $p = 0.0006$ ) and APP/PS1 ( $p < 0.0001$ ; Figure 5a). However, the total number of identified proteins in the EV<sup>ISF</sup> decreased with genotype, age, and A $\beta$  deposition, suggesting decreased EV<sup>ISF</sup> protein diversity (Figure 5b). The number of shared and unique EV<sup>ISF</sup> proteins among all four groups were examined (Figure 5c). 168 proteins were shared among all groups, revealing novel brain EV markers that may be specific to the hippocampus. 3-month WT mice had the following 20 unique EV<sup>ISF</sup> proteins: SNRPE, STRAP, PPP2CB, SRSF10, SARNP, PDIA3, PLEC, HSPA4L, FUBP1, CBX3, RPL37A, PSMD6, CCT4, RBMX, NME2, FH1, ELAVL1, RPS16, HSPA9, and PPIB. Interestingly, only two proteins were specific to 9-month WT EV<sup>ISF</sup>, TNNT3 and HMGB1. Surprisingly, no EV<sup>ISF</sup> proteins were unique to 3-month-old APP/PS1 mice. Five proteins were unique to the 9-month-old APP/PS1 group: GLUD1, FBXL21, ALDH2, PGLYRP1, and NGP. Comparisons of the proteins across the four groups showed decreased protein diversity due to both genotype and age in APP/PS1 compared to WT (Figure 5d). There were fewer unique proteins as well as an overall decrease in total protein number in APP/PS1 mice compared to WT beginning 3-months of age. This effect was potentiated in 9-month-old APP/PS1 mice, where a further reduction in unique proteins and protein number was observed compared to all groups. The greatest drop in protein diversity was observed in 9-month APP/PS1 compared to 3-month WT, which was commensurate with the greatest decrease in total protein number. Age-related changes in protein number were not as demonstrative, confirming that A $\beta$ -related pathology negatively impacts protein diversity more so than age. Thus, although protein concentration increased with both age and pathology, APP/PS1 genotype and plaque pathology decreased protein diversity compared to age-matched controls.

DAVID bioinformatics analyses were performed on EV<sup>ISF</sup> proteins from 3- and 9-month-old WT and APP/PS1 mice. Using DAVID, Gene Ontology (GO) terms for “Biological process” within each group were determined, and results with  $-\log(\text{FDR-value}) \geq 1.3$  were clustered into related categories including proteostasis, RNA processing, immune function, cellular trafficking, glucose metabolism, cell growth, wound healing, vascular function, DNA repair, circadian rhythms, cellular excitability, lipid metabolism, and epithelial development (Figure 5e). The number of biological processes that fell within each category were determined. Proteostasis, RNA processing, immune function, and cellular trafficking categories contained the greatest number of biological processes across all 4 groups. The number of proteostasis-related biological processes increased with age in WT compared to 3- or 9-month APP/PS1 groups. Both age and APP/PS1 genotype but not pathology reduced the number of RNA processing-related biological processes in EV<sup>ISF</sup>. Interestingly, an increase in the number of immune function-related biological processes was observed in 9-month WT mice when compared to 3-month WT, 3-month APP/PS1, and 9-month APP/PS1 groups. Age-related increases in the number of wound healing-, vascular function-, lipid metabolism-, and epithelial development-related biological processes were observed in both APP/PS1 and WT mice. Conversely, the number of biological processes related to DNA repair mechanisms specifically increased in APP/PS1 at 3-months but decreased with age regardless of genotype.

Bioinformatic analysis of EV<sup>ISF</sup> proteins reveals differences in biological pathways associated with genotype, age, and plaque pathology. DAVID bioinformatics analyses were performed on EV<sup>ISF</sup> proteins from 3- and 9-month-old WT and APP/PS1 mice. Using DAVID, Gene Ontology (GO) terms for “Biological process” within each group were determined, and results with  $-\log(\text{FDR-value}) \geq 1.3$  were clustered into related categories as described previously. 3-month APP/PS1 EV<sup>ISF</sup> had fewer total number of biological processes compared to 3-month WT (3 mo WT: 49; 3 mo APP/PS1: 36) (Figure S4a). While proteostasis related pathways were comparable between groups, pathways related to RNA processing were decreased in APP/PS1 mice compared to WT even at 3-months before amyloid plaque pathology was present (Figure S4a). This also corresponds with a decrease in protein diversity in 3-month-old APP/PS1 EV<sup>ISF</sup> compared to age-matched WT (see Figure 5b,d). On the other hand, the percentage of immune function-related biological processes increased in 3-month-old APP/PS1 versus 3-month WT EV<sup>ISF</sup> (3 mo WT: 14%; 3 mo APP/PS1: 19%) (Figure 6a). This suggests EV<sup>ISF</sup> signal and/or propagate an early inflammatory response in 3-month APP/PS1 before the presence of plaque pathology is detectable. DAVID analysis of the 3-month WT and APP/PS1 EV<sup>ISF</sup> revealed the top 10 GO terms for “Biological Process” and top 10 KEGG pathways while IPA revealed the top 10 canonical pathways. These results were grouped into the following categories: proteostasis, inflammation/immune, metabolism,



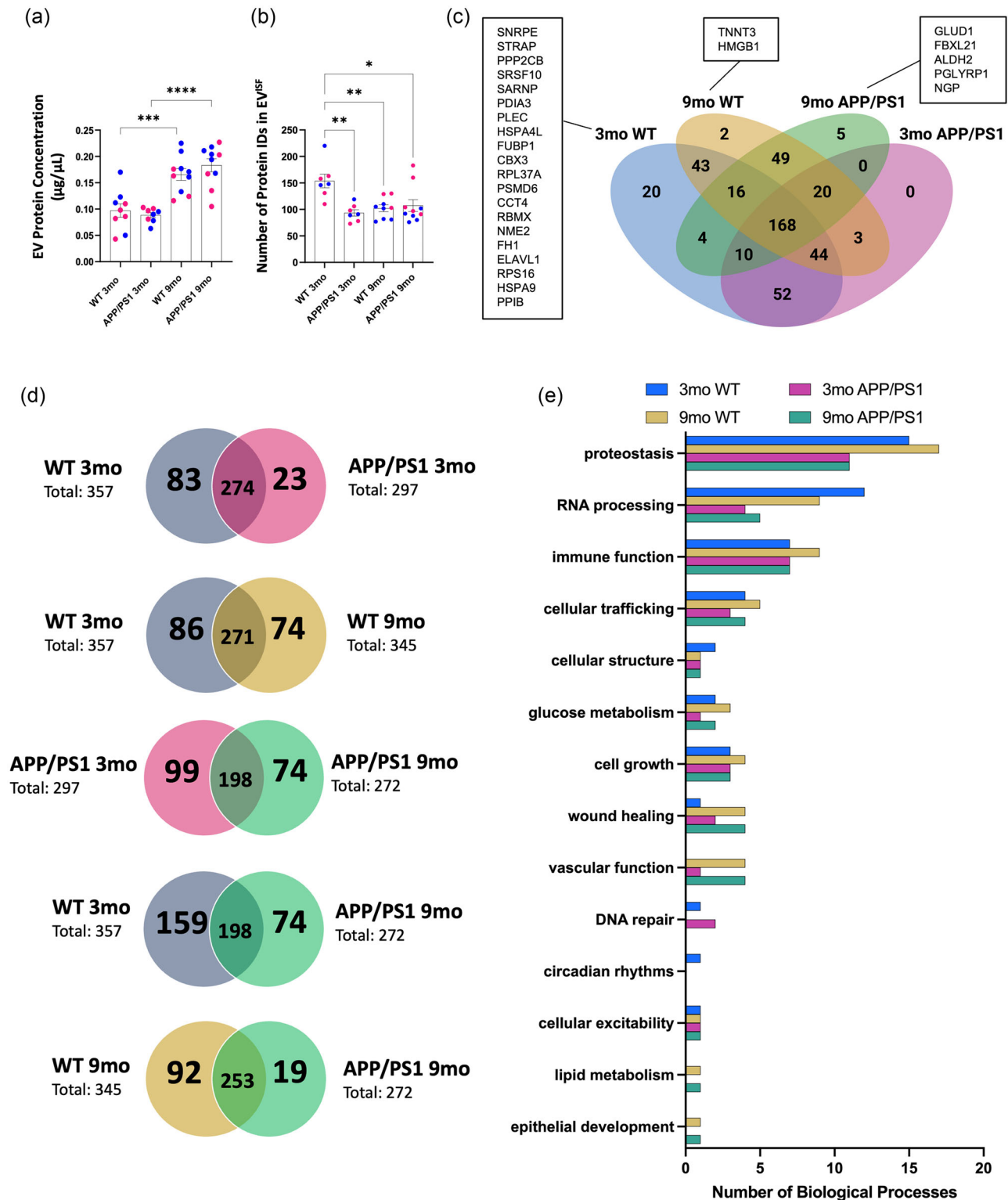


**FIGURE 5** Protein concentration increases with age and pathology while protein diversity decreases in EV<sup>ISF</sup>. (a) EV<sup>ISF</sup> protein concentration increased with age in both the WT ( $p = 0.0006$ ) and APP/PS1 mice ( $p < 0.0001$ ). (b) The number of unique protein IDs in EV<sup>ISF</sup> decreased with genotype ( $p = 0.0020$ ), age ( $p = 0.0054$ ), and pathology ( $p = 0.0113$ ) compared to 3-month WT. (c) Venn Diagram reveals unique and shared EV<sup>ISF</sup> proteins among all four groups: 3-month WT, 9-month WT, 3-month APP/PS1, and 9-month APP/PS1. (d) Venn diagrams of proteins unique to and shared between 3-month WT versus 3-month APP/PS1, 3-month WT versus 9-month WT, 3-month APP/PS1 versus 9-month APP/PS1, 3-month WT versus 9-month APP/PS1, and 9-month WT versus 9-month APP/PS1. Protein diversity decreased with genotype, age, and pathology. (E) DAVID analyses revealed changes in the number of biological processes within groups with age, genotype and pathology. One-way ANOVA, multiple comparisons Tukey's tests  $p < 0.05^*$ ,  $p < 0.01^{**}$ ,  $p < 0.001^{***}$ ,  $p < 0.0001^{****}$ .  $N = 7-10$  per group.

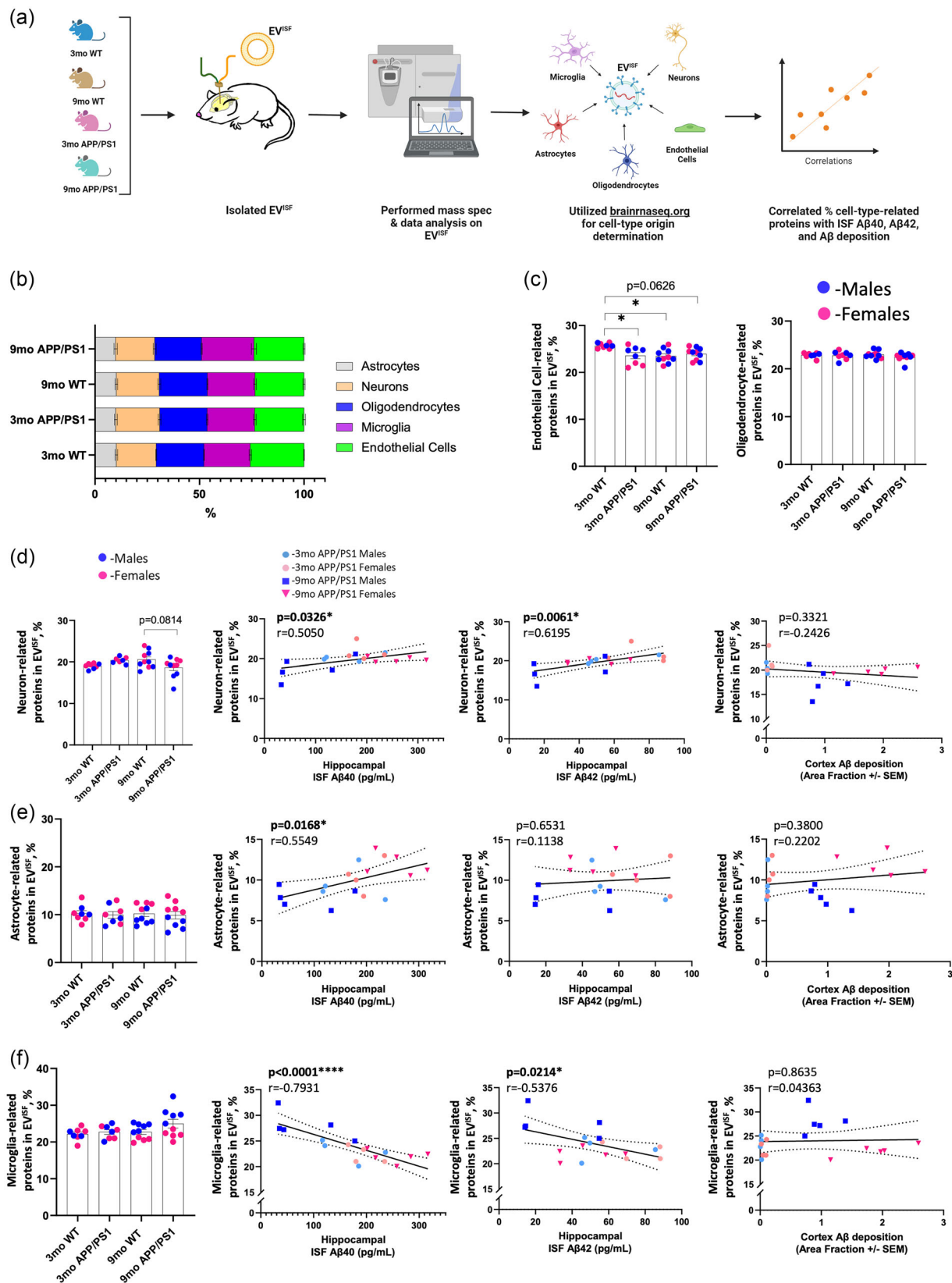


**FIGURE 6** A $\beta$  pathology and age modulate cell type-related EV<sup>ISF</sup> proteins. (a) Illustration of cell-sources of EV<sup>ISF</sup> proteins. (b) EV<sup>ISF</sup> proteins were searched in the brainrnaseq.org database (49) and were grouped according to their cell-source(s) per mouse. Percentages represent the average of each cell type-source per group. (c) In EV<sup>ISF</sup>, endothelial cell-related proteins decreased with APP/PS1 genotype ( $p = 0.0222$ ), age ( $p = 0.0110$ ), and A $\beta$  pathology ( $p = 0.0626$ ). There was no difference among groups for oligodendrocyte-related proteins in EV<sup>ISF</sup>. (d) Neuron-related proteins trended down with A $\beta$  pathology ( $p = 0.0814$ ) compared to 3-month APP/PS1. Percentage of neuron-related proteins correlated with ISF A $\beta$ 40 and A $\beta$ 42 levels but not A $\beta$  deposition in APP/PS1 mice. (e) The percentages of astrocyte-related proteins in EV<sup>ISF</sup> were unchanged across groups. However, they positively correlated with ISF A $\beta$ 40.

(Continues)

**FIGURE 6** (Continued)

(f) The percent of microglia-related proteins in EV<sup>ISF</sup> did not change among groups. However, they did negatively correlate with ISF A $\beta$ 40 and A $\beta$ 42 levels. Together, this demonstrates that microglial-, not the neuronal-, astrocyte-, or oligodendrocyte-, derived EV<sup>ISF</sup> proteome consistently changed with ISF A $\beta$  and A $\beta$  aggregation. One-way ANOVAs with Tukey multiple comparisons test.  $p < 0.05^*$  Endothelial:  $N = 8$ –10/group, Astrocyte:  $N = 8$ –10/group, Oligodendrocyte:  $N = 8$ –10/group, Neuron:  $N = 7$ –10/group. Microglia = 8–10/group. Correlation: Pearson  $r$  and two-tailed  $p$ -value:  $p < 0.05^*$ ,  $p < 0.0001^{****}$ .  $N = 18$ .

or structural integrity (Figure S4b). In the top 10 “Biological Process” results, RNA splicing, mRNA processing, formation of translation preinitiation complex, and translational initiation, all processes related to proteostasis, were present in 3-month WT EV<sup>ISF</sup> but not detected in 3-month APP/PS1 (Figure S4b). Conversely, the GO terms proteolysis involved in cellular protein catabolic process, positive regulation of protein localization to Cajal body, microtubule-based process, and intermediate filament organization were gained in the top 10 “Biological Process” results in 3-month APP/PS1 EV<sup>ISF</sup> (Figure S4b). This suggests that genotype alters proteostasis and structural integrity processes. For the top 10 KEGG pathway results, RNA transport and pentose phosphate pathways were present in 3-month WT but not detected in 3-month APP/PS1 EV<sup>ISF</sup> (Figure S4b). IPA results revealed that in the top 10 canonical pathways of 3-month APP/PS1 EV<sup>ISF</sup>, mTOR signalling and protein ubiquitination pathway were absent but 14-3-3-mediated signalling and gluconeogenesis I pathways were gained compared to 3-month WT (Figure 6b). These results demonstrate that EV<sup>ISF</sup> can detect and/or propagate proteostasis, inflammation/immune, and metabolic changes in WT and APP/PS1 as early as 3-months of age.

In 9-month APP/PS1 EV<sup>ISF</sup>, the total number of biological processes was lower compared to age-matched WT (Figure S5a). Many of the biological processes present in 9-month APP/PS1 and WT mice were shared, underscoring the important age-component of AD. In contrast, more pathways related to immunometabolism were present in APP/PS1 mice compared to WT at 9-month. For the top 10 “Biological Process” results, the GO terms regulation of translational initiation, formation of translation preinitiation complex, positive regulation of RNA polymerase II transcriptional preinitiation complex assembly, cell-cell adhesion, and positive regulation of telomerase RNA localization to Cajal body were lost from 9-month WT to 9-month APP/PS1 EV<sup>ISF</sup> (Figure S5b). However, 9-month APP/PS1 EV<sup>ISF</sup> gained protein folding, response to peptide hormone, acute-phase response, microtubule-based process, and muscle contraction (Figure S5b). The top 10 IPA canonical pathways revealed that regulation of eIF4 and p70S6K signalling, mTOR signalling, protein ubiquitination pathway, Huntington’s disease signalling, and FAT10 signalling pathway were lost in 9-month APP/PS1 EV<sup>ISF</sup> versus 9-month WT (Figure S5b). In contrast, 9-month APP/PS1 EV<sup>ISF</sup> gained the canonical pathways glucocorticoid receptor signalling, LXR/RXR Activation, acute phase response signalling, glycolysis I, and actin cytoskeleton signalling in the top 10 results versus age-matched WT (Figure S5b), suggesting changes in immunometabolism in APP/PS1 mice compared to age-matched controls.

### 3.5 | Percentages of cell type-related proteins in EV<sup>ISF</sup> are modulated by and correlate with ISF A $\beta$ levels in both sexes

Next, we explored whether EV<sup>ISF</sup> proteins originated from neurons, astrocytes, oligodendrocytes, microglia, and/or endothelial cells using the Barres Lab brainrnaseq.org database (Zhang et al., 2014) (Figure 6a; Table S1). If a protein was represented in more than one cell type, it was counted present for each cell type. Within each animal, the total number of times a particular cell type was identified was summed. The percentages of proteins from each cell type were calculated then represented as a percentage of the total pool for each of the four groups (Figure 6b). We found that cell type-specific changes in the EV<sup>ISF</sup> proteome were modulated by genotype, age, pathology, and sex. The percent of endothelial cell-related proteins decreased as a function of genotype ( $p = 0.0222$ ), age ( $p = 0.0110$ ), and A $\beta$  pathology ( $p = 0.0626$ ) in both male and female mice compared to 3-month WT (Figure 6c). Conversely, the percentage of oligodendrocyte-related proteins did not change across groups (Figure 6c). 9-month-old APP/PS1 mice trended towards a decrease ( $p = 0.0814$ ) in EV<sup>ISF</sup> neuron-related proteins compared to 9-month WT (Figure 6d). The percentage of neuron-related proteins in EV<sup>ISF</sup> positively correlated with ISF A $\beta$ 40 ( $p = 0.0326$ ,  $r = 0.5050$ ) and ISF A $\beta$ 42 ( $p = 0.0061$ ,  $r = 0.6195$ ) levels in APP/PS1 mice (Figure 6d). Interestingly, the percentage of neuron-related proteins in EV<sup>ISF</sup> did not correlate with A $\beta$  deposition (Figure 6d). This suggests that EV<sup>ISF</sup> neuronal proteins correlate with ISF A $\beta$  levels before amyloid plaque formation. While astrocyte-related proteins in EV<sup>ISF</sup> were unchanged between groups (Figure 6e), the percentage of astrocyte-related proteins in EV<sup>ISF</sup> positively correlated ( $p = 0.0168$ ,  $r = 0.5549$ ) with ISF A $\beta$ 40 levels. There was no correlation between astrocyte-EV<sup>ISF</sup> proteins and ISF A $\beta$ 42 or A $\beta$  deposition (Figure 6e). There was no change in the percentage of microglia-related proteins in EV<sup>ISF</sup> across groups (Figure 6f). However, microglia-EV<sup>ISF</sup> proteins negatively correlated with ISF A $\beta$ 40 ( $p < 0.0001$ ,  $r = -0.7931$ ) and ISF A $\beta$ 42 ( $p = 0.0214$ ,  $r = -0.5376$ ) levels but not with A $\beta$  deposition (Figure 6f).

### 3.6 | Microglia-related EV<sup>ISF</sup> proteins correlate with activated microglia (CD68<sup>+</sup>) in APP/PS1 in a sex-dependent manner

When our results were further stratified by sex, we observed sex-dependent effects of A $\beta$  pathology on microglia-related proteins in the EV<sup>ISF</sup> population. Specifically, the percentage of microglia-related proteins increased with the presence of plaque pathology in males but not females (Figure 7a). The percent of microglia-related proteins negatively correlated with ISF A $\beta$ 40 levels ( $p = 0.0163$ ,  $r = -0.7653$ ) only in APP/PS1 males. There was also a trend towards a negative correlation between microglia-related proteins and ISF A $\beta$ 42 levels only in APP/PS1 males ( $p = 0.0872$ ,  $r = -0.6006$ ; Figure 7a). However, the percentage of microglia-related proteins in EV<sup>ISF</sup> positively correlated with A $\beta$  deposition in male APP/PS1 ( $p = 0.0355$ ,  $r = 0.7008$ ; Figure 7a). In female mice, the percentage of microglia-related proteins in EV<sup>ISF</sup> did not change due to genotype, age, or pathology (Figure 7b). Moreover, microglia-related EV<sup>ISF</sup> proteins did not correlate with ISF A $\beta$ 40, ISF A $\beta$ 42 levels, or A $\beta$  deposition in APP/PS1 females (Figure 7b).

In addition to amyloid plaque burden, we also assessed the relationship between microglia-related proteins in EV<sup>ISF</sup> and disease-associated microglia (DAM), CD68<sup>+</sup> microglia. Consistent with previous results (Manocha et al., 2016, Takahashi et al., 2017), we observed an increase in CD68<sup>+</sup> staining in 9-month-old APP/PS1 mice compared to 3-month APP/PS1, 3-month WT, or 9-month WT mice (Figure 7c). There was no difference across groups for CD68<sup>+</sup> microglia staining in males (Figure 7c). However, female 9-month APP/PS1 had more CD68<sup>+</sup> microglia than 3-month WT ( $p = 0.0027$ ), 3-month APP/PS1 ( $p = 0.0035$ ), and 9-month WT ( $p = 0.0059$ ) mice (Figure 7c). CD68<sup>+</sup> staining positively correlated with A $\beta$  deposition in males ( $p = 0.0055$ ,  $r = 0.8657$ ) and trended towards a positive correlation with A $\beta$  deposition in females ( $p = 0.0875$ ,  $r = 0.06398$ ; Figure 7d). Interestingly, microglia-related proteins in EV<sup>ISF</sup> positively correlated with CD68<sup>+</sup> microglia staining in APP/PS1 males ( $p = 0.0395$ ,  $r = 0.7306$ ; Figure 7e). Surprisingly, microglia-related EV<sup>ISF</sup> proteins and CD68<sup>+</sup> staining did not correlate in female APP/PS1 (Figure 7e). This demonstrates that when levels of microglia activation in the brain increase in response to plaque pathology, levels of microglia-related proteins in the EV<sup>ISF</sup> of 9-month-old APP/PS1 males increase commensurately.

Finally, due to the differences seen between male and female microglia-related proteins, STRING analyses were performed on the EV<sup>ISF</sup> proteins from 9-month APP/PS1 male and female mice, separately (Figure 7f). The 9-month male and female APP/PS1 mice demonstrated unique and shared biological processes in their top 20 results. The unique biological pathways for 9-month-old male APP/PS1 EV<sup>ISF</sup> included many metabolic and vascular-associated processes (Figure 7f). On the other hand, the biological pathways found in 9-month-old female APP/PS1 EV<sup>ISF</sup> included metabolic, cellular response, and structural processes (Figure 7f). Interestingly, only 9-month-old female APP/PS1 mice had two AD-associated biological processes: 1) positive regulation of neurofibrillary tangle assembly and 2) negative regulation of amyloid fibril formation. These results were due to the presence of the AD-related proteins apolipoprotein E (APOE) and clusterin (CLU) in the 9-month female APP/PS1 EV<sup>ISF</sup> proteome, but not male (Figure 7f). Therefore, the sex-dependent, microglial protein differences found in EV<sup>ISF</sup> are associated with AD-related risk genes.

### 3.7 | Activated microglia in APP/PS1 mice differentially engage with amyloid plaques, sex-dependently

Since EV<sup>ISF</sup> revealed immunometabolic-related changes in their proteomes when A $\beta$  pathology was present, microglia and their association with amyloid plaques were assessed in 3-month and 9-month-old WT and APP/PS1 mice. Additionally, both homeostatic and activated, DAM microglia were examined across groups. Anterior cortex sections were co-stained for homeostatic microglia (Iba1), DAM microglia (CD68), and amyloid plaques (X34) (Figure 8a). APP/PS1 mice had greater plaque deposition when compared to WT ( $p = 0.0014$ ; Figure 8b). This genotype effect was driven by APP/PS1 females. 3-month APP/PS1 females had a trending increase in plaque deposition compared to age-matched WT ( $p < 0.054$ ) while 9-month APP/PS1 females had more amyloid plaques than WT mice ( $p = 0.0313$ ; Figure 8b). Plaque burden in APP/PS1 male mice was unchanged when compared to WT mice or APP/PS1 females (Figure 8b). Iba1 staining was unchanged across groups (Figure 8c).

On the other hand, CD68 staining revealed main effects in genotype ( $p = 0.0064$ ) and age ( $p = 0.0042$ ) as well as a genotype x age interaction ( $p = 0.0148$ ). CD68 increased in male APP/PS1 from 3-month to 9-month ( $p = 0.0218$ ; Figure 8d). 9-month APP/PS1 male mice also exhibited greater CD68 coverage when compared to 9-month WT males ( $p = 0.0460$ ; Figure 8d). However, CD68 did not change between 3-month and 9-months in APP/PS1 females (Figure 8d). Thus, activated, DAM microglia but not homeostatic microglia were increased only in male APP/PS1 mice when A $\beta$  pathology was present. Finally, the colocalization of X34, IBA1, and CD68 was assessed across groups to identify whether activated microglia were differentially recruited to amyloid plaques. Colocalization revealed main effects with genotype ( $p < 0.0001$ ), age ( $p < 0.0001$ ), and sex ( $p = 0.0259$ ). Further, there were main effects of genotype x age ( $p < 0.0001$ ), genotype x sex ( $p = 0.0259$ ), sex x age ( $p = 0.0041$ ), and sex x age x genotype ( $p = 0.0041$ ) interactions. Interestingly, APP/PS1 males demonstrated greater colocalization than females at 3-months ( $p = 0.0002$ ; Figure 8e,f). However, colocalization increased in APP/PS1 female mice with age and plaque pathology ( $p < 0.0001$ ).



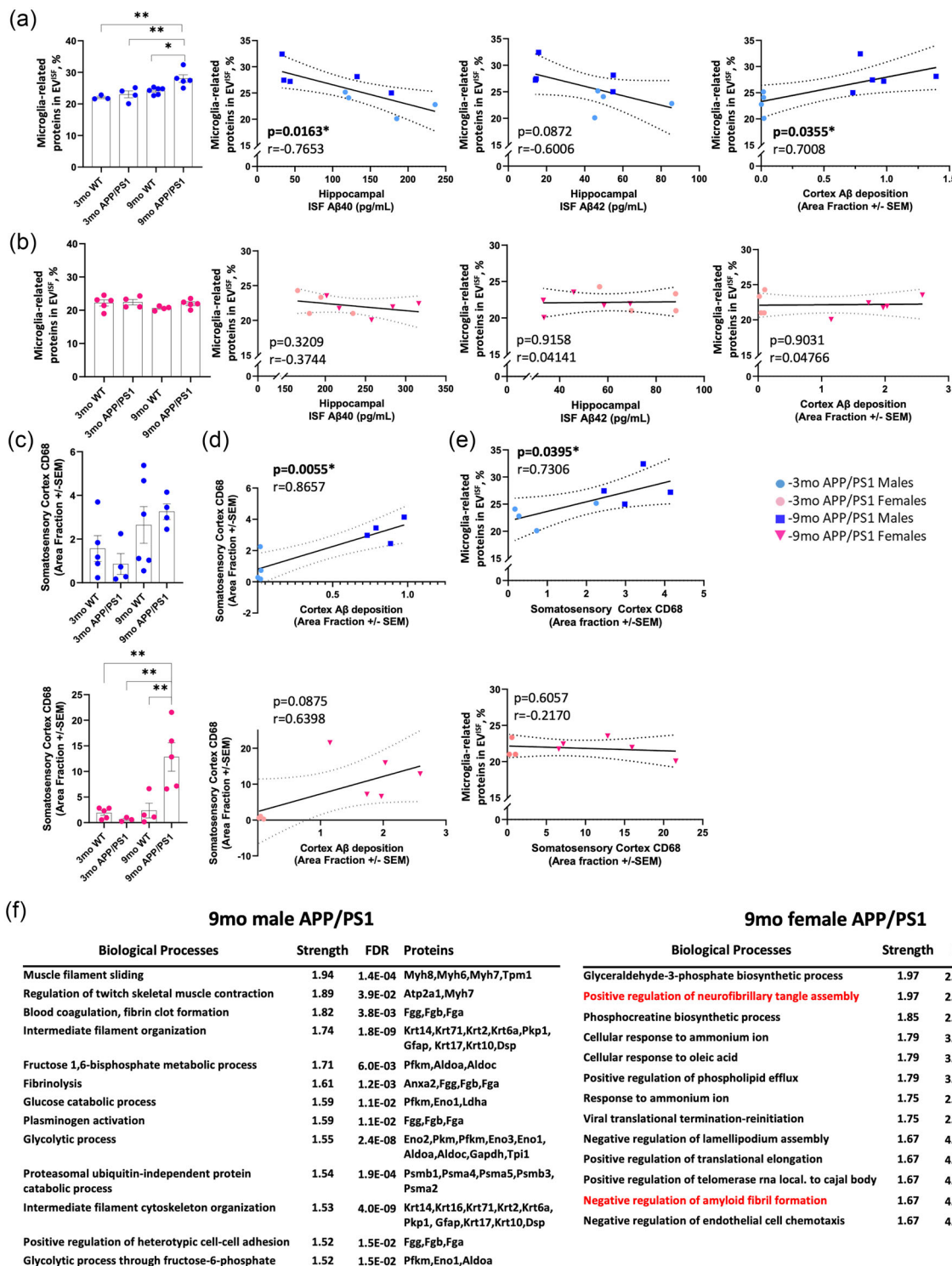


**FIGURE 7** Microglia-derived EV<sup>ISF</sup> proteins correlate with ISF Aβ, Aβ deposition, and microgliosis, sex-dependently, in APP/PS1. (a) EV<sup>ISF</sup> proteins were searched in the brainrnaseq.org database (49) and were grouped as described above. Percentages represent the average of each cell type source per group. When separated by sex, the percentage of EV<sup>ISF</sup> microglia-related proteins in males increased with age and pathology (Males: 3 mo WT vs. 9 mo APP/PS1:  $p = 0.0036$ , 3 mo APP/PS1 vs. 9 mo APP/PS1:  $p = 0.0074$ , 9 mo WT vs. 9 mo APP/PS1:  $p = 0.0208$ ). There was a negative correlation with ISF Aβ<sub>40</sub> levels and a positive correlation with Aβ deposition. There was a trending negative correlation with ISF Aβ<sub>42</sub>. (b) In contrast, there was no difference in the percentage of microglia-related proteins among groups in females. Also, microglia-proteins in EVs did not correlate with ISF Aβ<sub>40</sub>, ISF Aβ<sub>42</sub>, or Aβ deposition. (c) Only 9-month APP/PS1 females had increased CD68+ levels. (d) However, CD68+ microglia levels in APP/PS1 male mice correlated with Aβ deposition while females only had a positive trend. (e) The percentage of microglia-related proteins in EV<sup>ISF</sup> positively correlated with CD68+ microglia staining only in male APP/PS1. (f) Separate STRING analyses of 9-month APP/PS1 males and females revealed biological processes unique to each sex. Further, neurofibrillary tangle and amyloid-related biological processes in the top 20 results in females only. One-way ANOVAs with Tukey multiple comparison tests:  $p < 0.05^*$ ,  $p < 0.01^{**}$ ,  $p < 0.001^{***}$ ,  $p < 0.0001^{****}$ ,  $N = 3-10/\text{group}$ . Correlation: Pearson  $r$  and  $p$ -value:  $p < 0.05^*$ .

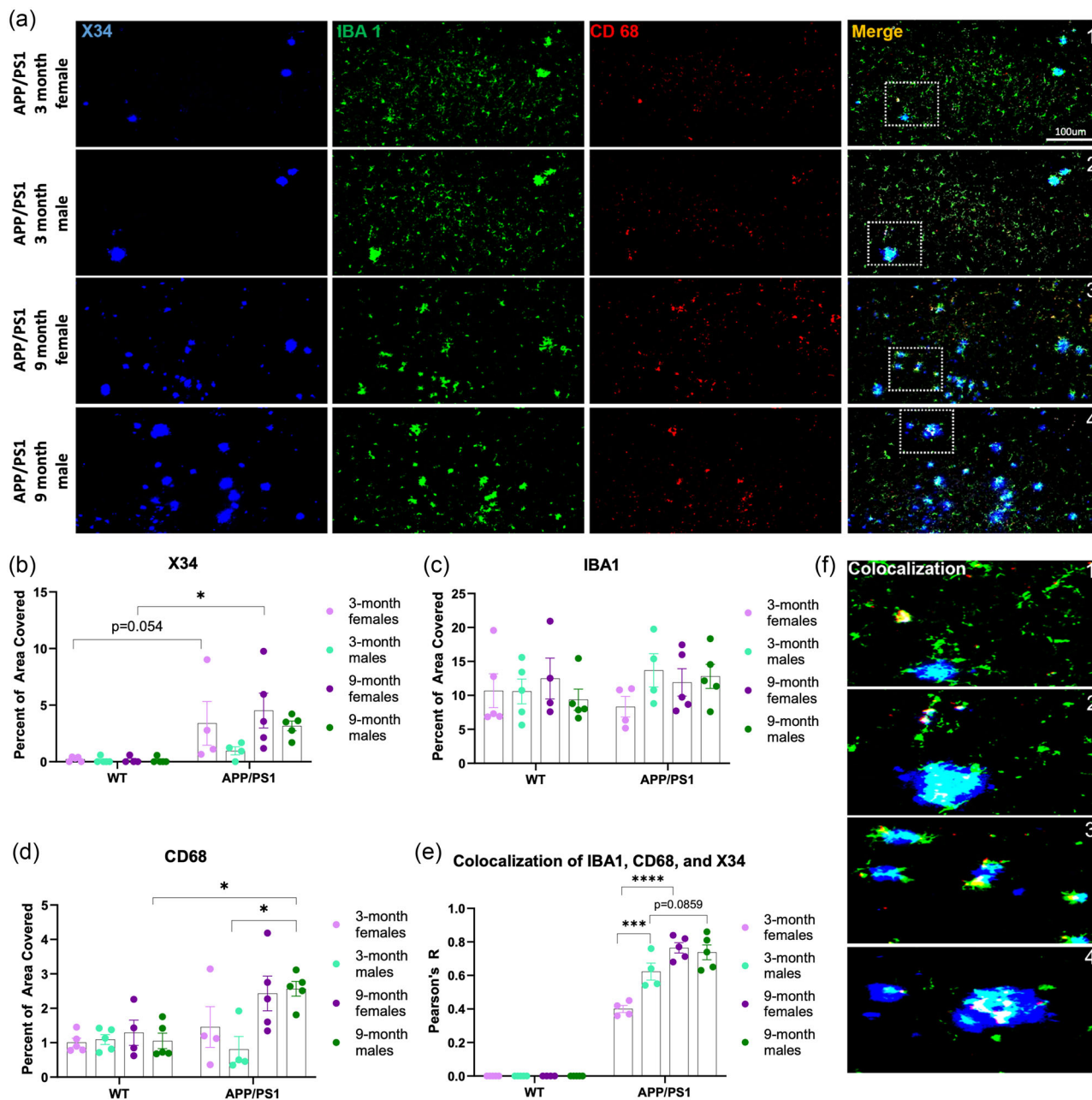


**FIGURE 8** Male and female microglia differentially associate with amyloid plaques. (a) Representative images of the anterior cortex taken from 3- and 9-month-old APP/PS1 mice. (b) Plaque coverage was quantified using X34. A main effect of genotype ( $p = 0.0014$ ) driven by female APP/PS1 mice was found. Post hoc analyses revealed 9-month female APP/PS1 mice had greater plaque coverage than WT ( $p = 0.0313$ ) with a similar trend at 3-months. (c) There were no statistical differences in macrophage coverage identified using IBA1. (d) Phagocytic activity was measured using CD68. There were main effects in genotype ( $p = 0.0064$ ) and age ( $p = 0.0042$ ) and a genotype x age interaction ( $p = 0.0148$ ). Post hoc analyses revealed that CD68 area coverage increased with age and plaque pathology in APP/PS1 male mice ( $p = 0.0218$ ). Further, 9-month APP/PS1 males had greater CD68 levels than 9-month WT ( $p = 0.0460$ ). (e) Colocalization analyses were performed to determine the involvement of microglia phagocytic activity in X34 deposition. There were main effects of genotype ( $p < 0.0001$ ), age ( $p < 0.0001$ ), and sex ( $p = 0.0259$ ). Three-way interaction revealed a main effect of genotype x age ( $p < 0.0001$ ), genotype x sex ( $p = 0.0259$ ), sex x age ( $p = 0.0041$ ), and sex x age x genotype ( $p = 0.0041$ ). Post hoc analyses revealed that 3-month APP/PS1 males had higher rates of colocalization than females ( $p = 0.0002$ ). Further, colocalization increased with age and plaque pathology in APP/PS1 females ( $p < 0.0001$ ) with a similar trend in APP/PS1 males. (f) Representative images of colocalization. Images are numbered 1–4 in relation to their original image in (a). Mixed-effects analyses with Tukey's multiple comparison tests:  $p < 0.05^*$ ,  $p < 0.01^{**}$ ,  $p < 0.001^{***}$ ,  $p < 0.0001^{****}$ ,  $N = 4$ –5/group.

while males had a trending increase ( $p = 0.0859$ ; Figure 8e). Thus, activated microglia differentially colocalize with amyloid plaques in a sex-dependent manner in APP/PS1 mice, where male mice show a greater number of plaque associated microglia early in life that is related to less amyloid pathology at late stages and a more robust EV<sup>ISF</sup> microglial proteome signature.

## 4 | DISCUSSION

We developed a novel and innovative method for examining the role of brain EVs in AD. This approach leveraged in vivo microdialysis as a way to isolate small EVs from the brain's ISF (EV<sup>ISF</sup>) in unanesthetized, freely moving mice. Not only were we able to circumvent potential limitations associated with current approaches, but we also made novel insights into the relationship between hippocampal EV<sup>ISF</sup> and the progression of AD. The EV field needs new approaches to isolate EVs from the brain's extracellular space without collecting ILVs or other extracellular nonvesicles (Théry et al., 2018). Historically, in vivo microdialysis has successfully collected proteins and metabolites directly from the brain's ISF (Cirrito et al., 2003, Holth et al., 2019, Macauley et al., 2015, Yamada et al., 2014, Yamada et al., 2011) yielding novel insights into how this dynamic pool is regulated. To date, A $\beta$ <sub>1-x</sub> (Bero et al., 2011, Cirrito et al., 2003, Macauley et al., 2015), A $\beta$ 38 (Hong et al., 2011), A $\beta$ 40 (Bero et al., 2011, Cirrito et al., 2003, Day et al., 2022, Hong et al., 2011), A $\beta$ 42 (Bero et al., 2011, Cirrito et al., 2003, Hong et al., 2011), tau (Holth et al., 2019, Yamada et al., 2011), ApoE (Ulrich et al., 2013), glucose (Day et al., 2022, Macauley et al., 2015), lactate (Bero et al., 2011, Macauley et al., 2015), and ethanol (Day et al., 2022) are all detectable in the ISF of mouse models of AD-related pathology. For the first time, we collected EV<sup>ISF</sup> via in vivo microdialysis and analysed their size, concentration, and proteome. Moreover, we investigated changes in EV<sup>ISF</sup> relative to age, sex, A $\beta$  pathology, and neuroinflammation. Using this approach, we found that while the total EV<sup>ISF</sup> concentration and protein concentration in EV<sup>ISF</sup> increases with pathology, the diversity of the EV<sup>ISF</sup> proteome decreased with A $\beta$  aggregation, specifically in proteins originating from neurons and endothelial cells. Interestingly, the increase in the EV<sup>ISF</sup> cargo proteins was largely due to microglial-derived proteins. Changes in the microglial EV<sup>ISF</sup> proteome were sexually dimorphic and associated with a differential response of plaque associated microglia. We found that the female APP/PS1 mice have more amyloid plaques, less plaque associated microglia, and a less robust- and diverse- EV<sup>ISF</sup> microglial proteome. Pathway analysis on the EV<sup>ISF</sup> proteome from female APP/PS1 mice showed two pro-Alzheimer's related pathways driven by two AD associated risk proteins, APOE and CLU, that are known to promote A $\beta$  aggregation (DeMattos et al., 2002, Holtzman, 2004). These proteins were not detected in EV<sup>ISF</sup> from the male APP/PS1 mice. Together, we not only developed a novel method of collecting EVs from the hippocampal ISF, but also demonstrated a sexually dimorphic response of microglia to A $\beta$  pathology that is related to the microglial EV<sup>ISF</sup> proteome. These observations not only suggest a role for EVs in microglia-amyloid plaque interactions, but also has implications for EV-based biomarker development which historically focuses on neuronal- or astrocyte-derived EVs to stage or diagnosis AD.

Our novel in vivo microdialysis approach is important because it avoids caveats from existing methods. To date, brain-EVs are isolated from postmortem, not live, brain tissue. While this includes the study of brain-EVs from humans, rodent models, and nonhuman primates, postmortem analyses have caveats. The postmortem interval can alter RNA expression and integrity (Ferreira et al., 2018), shift brain metabolism (Juras et al., 2023), and accelerate protein degradation (Blair et al., 2016). Thus, postmortem tissue changes may affect brain-derived EVs by causing artifactual changes in the EV cargo that would be absent if isolated from a live brain. Several brain tissue-derived EV techniques use harsher isolation protocols, resulting in potential intracellular and nonvesicular contamination (Banigan et al., 2013, Gallart-Palau et al., 2016, Perez-Gonzalez et al., 2012, Pérez-González et al., 2017, Vella et al., 2017, Yelamanchili et al., 2015). Since ILVs retain many of the same markers as secreted EVs, it is hard to delineate whether an EV pool is found intracellularly or extracellularly with current techniques. In vivo microdialysis collection of EV<sup>ISF</sup> circumvents these caveats. Our approach also allows us to explore EVs from a specific brain region vulnerable to AD pathology during amyloid plaque formation (Braak et al., 1993). Sampling brain-derived EVs from biofluids like blood or CSF represents a heterogeneous pool of brain-derived EVs that may or may not have originated from regions impacted by AD-related pathology. Additionally, samples are traditionally examined distal to the brain in humans, monkeys, and rodents which relies on intact transport and clearance mechanisms, which are dysfunctional in AD and other CNS diseases. Despite advances in the EV field, it is still difficult to isolate and compare EVs from specific brain regions even in postmortem tissue (Huang et al., 2020, Ruan et al., 2020, Vassileff et al., 2020, Vella et al., 2017). Because of the limited number of human or nonhuman primate samples, often only one brain region from a few samples can be studied at a time. While more brain regions and a greater sample size can be employed using rodent models, size constraints limit region-specific isolation of brain-EVs with current methods. An entire brain hemisphere, a whole brain, or pooled mouse brains are generally required for EV isolation (D'Acunzo et al., 2022, Harrison et al., 2016, Hurwitz et al., 2018, Muraoka et al., 2020, Perez-Gonzalez et al., 2012). Thus, differences in EVs from different brain regions are missed. This is imperative for studying CNS disease since not all brain regions are uniformly impacted by disease or undergo pathological changes at the same rate. In contrast, changes in peptides, proteins, or metabolites due to pathology, age, or pharmacological intervention can be measured in the ISF of specific brain regions using in vivo microdialysis (Harris et al., 2016, Macauley et al., 2015, Roh et al., 2012, Stanley et al., 2016). We have now expanded this approach to measure changes in EVs as it relates to AD-related pathology.

Given what is well established in the EV field, several of our study's key findings were unexpected. First, our approach revealed sex-dependent changes in EV<sup>ISF</sup> concentration due to age not observed in previous studies. EV<sup>ISF</sup> concentration increased as male mice aged but not females (Figure 3f). This is in contrast to a plasma-EV study that found EV concentration decreased with age (Eitan et al., 2017). These changes could reflect age- or pathology-related changes in clearance mechanisms that plague most



CNS diseases, including AD. We also found protein concentration within hippocampal EV<sup>ISF</sup> increased with age in WT mice (Figure 5a) while protein diversity remained the same (Figure 5b,d). In contrast with hippocampal EV<sup>ISF</sup>, the contents of plasma-EVs decreased with age (Lazo et al., 2021). Interestingly, the number of proteostasis-related biological processes increased as the mice aged in our EV<sup>ISF</sup> (Figure 5e). These results agree with studies demonstrating that aging affects proteostasis via alterations in protein synthesis, degradation, chaperones, the ubiquitin-proteasome system, and autophagy (Kaushik & Cuervo, 2015). Next, we explored how EV<sup>ISF</sup> protein concentration and diversity changed with amyloid pathology. Here, we observed an age-dependent increase in EV<sup>ISF</sup> protein concentration, but a striking decrease in protein diversity in the 9-month APP/PS1 mice (Figure 5a,b,d). We hypothesized that since changes in protein synthesis, trafficking, degradation, and clearance are all affected in AD, changes in EV<sup>ISF</sup> proteome reflect this. Indeed, the number of proteostasis-related biological processes as well as the number of proteostasis-related pathways decreased with APP/PS1 genotype and A $\beta$  deposition compared to age-matched WT (Figure 5e, Figures S4b, and S5b). These results agree with the literature demonstrating that proteostasis is dysregulated in aging and AD (Hernández-Ortega et al., 2016; Koga et al., 2011; Powers et al., 2009). Thus, AD-related changes in proteostasis appear to be modulating protein diversity, biological processes, and pathways within hippocampal EV<sup>ISF</sup> population.

Next, we demonstrate that the EV<sup>ISF</sup> proteome changes in a cell type-specific manner in vivo despite a global increase in EV<sup>ISF</sup> protein concentration with age. While percentage of oligodendrocyte- and astrocyte-related proteins in EV<sup>ISF</sup> are unchanged with genotype, age, or A $\beta$  deposition (Figure 6c), we did see that endothelial-, neuronal-, and microglial-associated cargo proteins were affected by age, sex, or genotype. For example, endothelial cell-related proteins in hippocampal EV<sup>ISF</sup> decreased with genotype and age and had a trending decrease as mice developed amyloid plaques (Figure 6c). However, changes in endothelial-related proteins in EV<sup>ISF</sup> did not correlate with changes in ISF A $\beta$ 40, ISF A $\beta$ 42, or amyloid pathology. In humans, endothelial cell-EVs increased with disease in plasma from AD patients (Aharon et al., 2020). This difference could be due to the fact that vascular-derived EVs are secreted into blood vessel lumen, not brain parenchyma, as the disease develops. Therefore, changes in protein abundance would be reflected in the plasma, not ISF EV pool. Conversely, it could suggest decreases in the vascular-EV proteome may be more important to pursue as an AD biomarker when staging disease progression. While astrocyte-related proteins in EV<sup>ISF</sup> were unchanged across groups (Figure 6e), we did find a positive correlation between astrocyte-related proteins in EV<sup>ISF</sup> and ISF A $\beta$ 40 levels. It is also interesting that astrocyte-related proteins in EV<sup>ISF</sup> correlate with ISF A $\beta$ 40, but not ISF A $\beta$ 42 or amyloid pathology. ISF A $\beta$ 40 is the more abundant species of A $\beta$  and less aggregatory prone compared to A $\beta$ 42 (Holtzman et al., 2011; Iwatsubo et al., 1994; Jarrett et al., 1993; Schindler et al., 2018), but also highly regulated by changes in excitatory neurotransmission (Cirrito et al., 2003; Cirrito et al., 2005; Kamenetz et al., 2003). The development of A $\beta$  deposition can modulate levels of A $\beta$  in the ISF. When in vivo microdialysis was performed on transgenic mice that develop amyloid plaque pathology, levels of ISF A $\beta$ 40 and A $\beta$ 42 all decreased with the development of A $\beta$  aggregation and amyloid plaques (Hong et al., 2011). In another mouse model of AD-related pathology, levels of ISF A $\beta$ 40 and A $\beta$ 42 in young mice predicted A $\beta$  deposition in multiple brain regions, including hippocampus (Bero et al., 2011). Thus, as amyloid plaque pathology develops in the brain, levels of both ISF A $\beta$ 40 and A $\beta$ 42 decrease. We hypothesize the relationship between ISF A $\beta$ 40 and astrocyte-related proteins in EV<sup>ISF</sup> reflects astrocyte-neuron cooperation in the healthy brain, which is lost with the onset of A $\beta$  aggregation. In fact, when examining the astrocyte-derived EV<sup>ISF</sup> proteome in 9-month APP/PS1 mice using STRING, there is a shift towards pathways involved in A $\beta$ /tau aggregation, cellular metabolism, and inflammation (data not shown). While this suggests that the EV pool of astrocyte-related proteins is stable across genotype, sex, and age, exploring how specific proteins change in astrocyte-derived proteins holds promise as AD biomarkers in agreement with previous studies (Goetzl et al., 2016). In our EV<sup>ISF</sup> population, neuron-related proteins had a trending decrease with A $\beta$  deposition (Figure 6d) but positive correlations with ISF A $\beta$ 40 and ISF A $\beta$ 42 levels. Similar to the findings with the EV<sup>ISF</sup> astrocyte-derived proteome, this suggests that neuronal activity drives EV<sup>ISF</sup> release in a manner similar to A $\beta$ <sub>1-x</sub> (Bero et al., 2011; Cirrito et al., 2008; Cirrito et al., 2005). It also suggests that as A $\beta$ 40 and A $\beta$ 42 levels drop in the ISF, which occurs during A $\beta$  aggregation (Fagan et al., 2006), neuron-derived proteins in EV<sup>ISF</sup> also decrease. This is consistent with previous studies that found neuronal-related markers in brain tissue-EVs were decreased in AD patients compared to controls (Muraoka et al., 2020; Ruan et al., 2020). However, many studies still focus on changes in neuronal-derived EVs or exosomes as a biomarker of AD pathology. If less neuronal-derived proteins are synthesized, packaged, or trafficked in EVs in regions undergoing degeneration, then neuronal-derived EVs may not be the most attractive biomarker in AD. It would be interesting to explore the relationship between neuronal-derived EVs and AD further.

The most interesting results from our study were related to EV<sup>ISF</sup> microglia-related proteins (Figure 7). First, prior to the formation of amyloid plaques, EV<sup>ISF</sup> from 3-month APP/PS1 mice had a greater number of inflammation-related pathways compared to 3-month WT (Figure S4b). Following A $\beta$  deposition, there are more immunometabolic-related canonical pathways in EV<sup>ISF</sup> compared to controls (Figure S5b), highlighting the role of neuroinflammation in AD as well as other neurodegenerative diseases (Casetto et al., 2022; Sala Frigerio et al., 2019; Shippy & Ulland, 2020). Next, increases in the EV<sup>ISF</sup> microglia-related proteins were negatively correlated with ISF A $\beta$ 40 and ISF A $\beta$ 42, suggesting that an increase in EV<sup>ISF</sup> microglial-proteins is associated with drops in both ISF A $\beta$ 40 and A $\beta$ 42 or the development of A $\beta$  aggregation (Figure 7f). When separated by sex, EV<sup>ISF</sup> microglia-related proteins increased with A $\beta$  deposition in male APP/PS1 mice and correlated with ISF A $\beta$ 40, ISF A $\beta$ 42, and, most interestingly, cortical A $\beta$  deposition in male mice (Figure 7a). We demonstrate that as early as 3-months of age when A $\beta$  starts to aggregate, CD68+ microglia colocalize more strongly with amyloid plaques in male mice compared to females



(Figure 8e). This is despite more total CD68+ microglia in female mice (Casaletto et al., 2022, Gallagher et al., 2013, Lynch, 2022, Sala Frigerio et al., 2019). We also see that EV<sup>ISF</sup> microglia-related proteins are positively correlated with amyloid plaques, but only in male mice, which also have less amyloid pathology than females. Comparing the total EV<sup>ISF</sup> proteome at 9-months, pathway analysis revealed two AD-related pathways related to neurofibrillary tangle assembly and amyloid fibril formation are driven by the AD-related proteins and pro-A $\beta$  aggregatory proteins, APOE and CLU, but only in female mice. Our studies demonstrate a sexually dimorphic response of microglia to amyloid plaques which may offer one explanation to why there is a differential risk for males and females in AD. Moreover, the EV<sup>ISF</sup> microglial proteome differs by sex, shedding light on the sex-dependent role for microglia proteins and EVs in AD.

Given the strong relationship between EV<sup>ISF</sup> microglia-related proteins and A $\beta$ , this suggests that microglial-derived EVs could be an attractive, early biomarker of A $\beta$ -related changes in the brain. Previous studies demonstrate that microglial-derived EVs can transport pathological tau and A $\beta$  (Asai et al., 2015, Ruan et al., 2020, Ruan et al., 2020). Microglia can uptake EVs from the extracellular space, serving as a brain clearance mechanism for A $\beta$  (Yuyama et al., 2012). Brain-EVs isolated from postmortem AD models demonstrate that DAM microglia can excessively secrete EVs in the brain in the presence of AD-related pathology (Clayton et al., 2021) and brain tissue-EVs express an enrichment of DAM proteins (Muraoka et al., 2021). To date, few studies have explored sexually dimorphic response of microglia to AD-related pathology and whether microglial derived-EVs are involved, which may offer one explanation to why there is a differential risk for males and females in AD. Our data provides mechanistic support for epidemiological studies that females are at greater risk for AD compared to males. Thus, our technique for hippocampal EV<sup>ISF</sup> collection reveals previously undescribed changes in cell type-specific proteins with age, sex, genotype, and A $\beta$  deposition. Moreover, it suggests that microglial-derived EVs hold promise for staging the progression of AD. Further examination of brain-EVs in vivo provides a unique opportunity to better understand the role brain-derived EVs, particularly microglial-derived EVs, play in AD as well as their role as potential biomarkers.

## 5 | LIMITATIONS

There are several limitations to our current study that need to be discussed. First, one caveat to this study is that we did not isolate EVs from postmortem brain tissue in conjunction with our in vivo hippocampal EV<sup>ISF</sup> isolation method. Thus, we were unable to directly compare our in vivo EV isolation technique with previously published postmortem tissue isolation methods. This is because no current EV tissue isolation methods allow for isolation of EVs from specific brain regions of individual mice. All current methods require either pooling of brain regions from several mice or utilization of an entire hemisphere or whole brain from one mouse (D'Acunzo et al., 2022, Harrison et al., 2016, Hurwitz et al., 2018, Muraoka et al., 2020, Perez-Gonzalez et al., 2012). Similarly, we were unable to collect CSF-EVs from our mice without pooling CSF samples from multiple mice due to the low volume of collectable CSF from individual mice (Vandendriessche et al., 2021, Yuyama et al., 2015). Thus, at this time, we were unable to directly isolate and compare our in vivo hippocampal EV<sup>ISF</sup> to EVs isolated from postmortem hippocampal tissue or in vivo CSF from the same mouse. Nevertheless, we did compare our EV<sup>ISF</sup> to previously published proteomic results from postmortem brain tissue of both mice and humans for validation. As EV tissue isolation methods become more refined, future studies should examine the differences in EVs isolated from in vivo and postmortem brain tissue. Since ISF volume was also a limiting factor, additional characterization of the particles found in hippocampal ISF, beyond EVs, could not be accomplished in this study. Therefore, we cannot rule out that our EV<sup>ISF</sup> population has protein aggregates or particles that do not fit the criteria of EVs. Similarly, we cannot rule out with our current methodology that any protein or antibody aggregation or micelles of dye in various assays is responsible for a higher signal-to-noise ratio. Therefore, more method development is needed to generate better EV isolation for low volume samples.

## 6 | CONCLUSION

In conclusion, we developed and validated a novel approach using in vivo microdialysis to isolate sEVs from the ISF of the live brain to better understand the role of brain-derived EVs in AD. Our work builds upon the current EV and AD literature to capture how the dynamic, in vivo pool of EV<sup>ISF</sup> changes with AD pathogenesis in a brain region vulnerable to disease. EV<sup>ISF</sup> are altered with age. They reveal proteostasis changes that are modulated by the presence of A $\beta$  deposition. More inflammatory- and immune-related pathways appear in EV<sup>ISF</sup> with APP/PS1 genotype and plaque pathology compared to WT. Microglia-related proteins are sex-dependently increased in male 9-month APP/PS1 EV<sup>ISF</sup>. Thus, microglial contents of EV<sup>ISF</sup> may be moderating a beneficial immunometabolic response that could be driving the sex differences seen not only in APP/PS1 mice but also in humans with AD (Casaletto et al., 2022, Guillot-Sestier et al., 2021). Studying EV<sup>ISF</sup> will further elucidate the roles of EVs, microglia, and sex-differences in AD pathology.

## AUTHOR CONTRIBUTIONS

S.L.M. and G.D. conceived of the study. S.L.M., G.D., and M.C.P. contributed to study design. M.C.P., S.D.K., Y.S., A.K., S.S., S.C.G., S.V., M.A., C.M.C., J.A.S., and J.L. performed experiments. M.C.P., S.D.K., and S.C.G. performed data analysis and data interpretation. M.C.P., S.L.M., and G.D. wrote the manuscript. All authors discussed the results and commented on the manuscript.

## ACKNOWLEDGEMENTS

We would like to thank Dr. David Holtzman for the generous gifts of A $\beta$  antibodies. We would like to acknowledge the following grants: Wake Forest Alzheimer's Disease Research Center pilot and R01AG061805 (G.D., S.L.M.), P30AG072947 (S.L.M.), K01AG050719 (S.L.M.), R01AG068330 (S.L.M.), BrightFocus Foundation A20201775S (S.L.M.), Averill Foundation (S.L.M.), F31AG071119 (M.P.), and Wake Forest Baptist Comprehensive Cancer Center Proteomics and Metabolomics Shared Resource, supported by the National Cancer Institute's Cancer Center Support Grant award number P30CA012197.

## CONFLICT OF INTEREST STATEMENT

S.L.M. served as a consultant for Denali Therapeutics, which has no influence or contribution to the work presented in this manuscript. G.D. is the founder of LiBiCo, which has no influence or contribution to the work presented in this manuscript.

## DATA AVAILABILITY STATEMENT

The datasets used, produced, and/or analysed during the current study are available from the corresponding author on reasonable request. Of note, all data generated or analysed during this study are included in this published article. All proteomic datasets will be open access.

## ORCID

Gagan Deep  <https://orcid.org/0000-0003-4445-8796>

Shannon L. Macauley  <https://orcid.org/0000-0002-4292-2703>

## REFERENCES

- Aharon, A., Spector, P., Ahmad, R. S., Horrany, N., Sabbach, A., Brenner, B., & Aharon-Peretz, J. (2020). Extracellular vesicles of Alzheimer's disease patients as a biomarker for disease progression. *Molecular Neurobiology*, 57(10), 4156–4169.
- Alvarez, X. A., Winston, C. N., Barlow, J. W., Sarsoza, F. M., Alvarez, I., Aleixandre, M., Linares, C., García-Fantini, M., Kastberger, B., Winter, S., & Rissman, R. A. (2022). Modulation of amyloid- $\beta$  and tau in Alzheimer's disease plasma neuronal-derived extracellular vesicles by cerebrolysin® and donepezil. *Journal of Alzheimer's disease*, 90(2), 705–717.
- Asai, H., Ikezu, S., Tsunoda, S., Medalla, M., Luebke, J., Haydar, T., Wolozin, B., Butovsky, O., Kügler, S., & Ikezu, T. (2015). Depletion of microglia and inhibition of exosome synthesis halt tau propagation. *Nature Neuroscience*, 18(11), 1584–1593.
- Banigan, M. G., Kao, P. F., Kozubek, J. A., Winslow, A. R., Medina, J., Costa, J., Schmitt, A., Schneider, A., Cabral, H., Cagsal-Getkin, O., Vanderburg, C. R., & Delalle, I. (2013). Differential expression of exosomal microRNAs in prefrontal cortices of schizophrenia and bipolar disorder patients. *PLoS One*, 8(1), e48814.
- Bateman, R. J., Wen, G., Morris, J. C., & Holtzman, D. M. (2007). Fluctuations of CSF amyloid-beta levels: Implications for a diagnostic and therapeutic biomarker. *Neurology*, 68(9), 666–669.
- Bero, A. W., Yan, P., Roh, J. H., Cirrito, J. R., Stewart, F. R., Raichle, M. E., Lee, J. M., & Holtzman, D. M. (2011). Neuronal activity regulates the regional vulnerability to amyloid- $\beta$  deposition. *Nature Neuroscience*, 14(6), 750–756.
- Blair, J. A., Wang, C., Hernandez, D., Siedlak, S. L., Rodgers, M. S., Achar, R. K., Fahmy, L. M., Torres, S. L., Petersen, R. B., Zhu, X., Casadesus, G., & Lee, H. G. (2016). Individual case analysis of postmortem interval time on brain tissue preservation. *PLoS One*, 11(3), e0151615.
- Braak, H., Braak, E., & Bohl, J. (1993). Staging of Alzheimer-related cortical destruction. *European Neurology*, 33(6), 403–408.
- Brás, I. C., Khani, M. H., Riedel, D., Parfentev, I., Gerhardt, E., van Riesen, C., Urlaub, H., Gollisch, T., & Outeiro, T. F. (2022). Ectosomes and exosomes modulate neuronal spontaneous activity. *Journal of Proteomics*, 269, 104721.
- Buzas, E. I. (2023). The roles of extracellular vesicles in the immune system. *Nature Reviews Immunology*, 23, 236–250.
- Casaleto, K. B., Nichols, E., Aslanyan, V., Simone, S. M., Rabin, J. S., La Joie, R., Brickman, A. M., Dams-O'Connor, K., Palta, P., Kumar, R. G., George, K. M., Satizabal, C. L., Schneider, J., & Pa, J. (2022). Sex-specific effects of microglial activation on Alzheimer's disease proteinopathy in older adults. *Brain*, 145(10), 3536–3545.
- Cha, D. J., Mengel, D., Mustapic, M., Liu, W., Selkoe, D. J., Kapogiannis, D., Galasko, D., Rissman, R. A., Bennett, D. A., & Walsh, D. M. (2019). miR-212 and miR-132 Are downregulated in neurally derived plasma exosomes of Alzheimer's patients. *Frontiers in Neuroscience*, 13, 1208.
- Cheng, L., Sharples, R. A., Scicluna, B. J., & Hill, A. F. (2014). Exosomes provide a protective and enriched source of miRNA for biomarker profiling compared to intracellular and cell-free blood. *Journal of Extracellular Vesicles*, 3, 23743. <https://doi.org/10.3402/jev.v3.23743>
- Cheng, L., Vella, L. J., Barnham, K. J., McLean, C., Masters, C. L., & Hill, A. F. (2020). Small RNA fingerprinting of Alzheimer's disease frontal cortex extracellular vesicles and their comparison with peripheral extracellular vesicles. *Journal of Extracellular Vesicles*, 9(1), 1766822.
- Choi, D. S., Kim, D. K., Kim, Y. K., & Ghoo, Y. S. (2013). Proteomics, transcriptomics and lipidomics of exosomes and ectosomes. *Proteomics*, 13(10–11), 1554–1571.
- Cirrito, J. R., Kang, J. E., Lee, J., Stewart, F. R., Verges, D. K., Silverio, L. M., Bu, G., Mennerick, S., & Holtzman, D. M. (2008). Endocytosis is required for synaptic activity-dependent release of amyloid-beta in vivo. *Neuron*, 58(1), 42–51.
- Cirrito, J. R., May, P. C., O'Dell, M. A., Taylor, J. W., Parsadanian, M., Cramer, J. W., Audia, J. E., Nissen, J. S., Bales, K. R., Paul, S. M., DeMattos, R. B., & Holtzman, D. M. (2003). In vivo assessment of brain interstitial fluid with microdialysis reveals plaque-associated changes in amyloid-beta metabolism and half-life. *The Journal of Neuroscience*, 23(26), 8844–8853.
- Cirrito, J. R., Yamada, K. A., Finn, M. B., Sloviter, R. S., Bales, K. R., May, P. C., Schoepp, D. D., Paul, S. M., Mennerick, S., & Holtzman, D. M. (2005). Synaptic activity regulates interstitial fluid amyloid-beta levels in vivo. *Neuron*, 48(6), 913–922.

- Clayton, K., Delpech, J. C., Herron, S., Iwahara, N., Ericsson, M., Saito, T., Saido, T. C., Ikezu, S., & Ikezu, T. (2021). Plaque associated microglia hyper-secrete extracellular vesicles and accelerate tau propagation in a humanized APP mouse model. *Molecular Neurodegeneration*, 16(1), 18.
- Cohn, W., Melnik, M., Huang, C., Teter, B., Chandra, S., Zhu, C., McIntire, L. B., John, V., Gyllys, K. H., & Bilousova, T. (2021). Multi-omics analysis of microglial extracellular vesicles from human Alzheimer's disease brain tissue reveals disease-associated signatures. *Frontiers in Pharmacology*, 12, 766082.
- Colombo, M., Raposo, G., & Théry, C. (2014). Biogenesis, secretion, and intercellular interactions of exosomes and other extracellular vesicles. *Annual Review of Cell and Developmental Biology*, 30, 255–289.
- Console, L., Scalise, M., & Indiveri, C. (2019). Exosomes in inflammation and role as biomarkers. *Clinica chimica acta; International Journal of Clinical Chemistry*, 488, 165–171.
- D'Acunzo, P., Kim, Y., Ungania, J. M., Pérez-González, R., Goulbourne, C. N., & Levy, E. (2022). Isolation of mitochondria-derived mitovesicles and subpopulations of microvesicles and exosomes from brain tissues. *Nature Protocols*, 17(11), 2517–2549.
- Datta Chaudhuri, A., Dasgheyb, R. M., DeVine, L. R., Bi, H., Cole, R. N., & Haughey, N. J. (2020). Stimulus-dependent modifications in astrocyte-derived extracellular vesicle cargo regulate neuronal excitability. *Glia*, 68(1), 128–144.
- Delgado-Peraza, F., Noguera-Ortiz, C. J., Volpert, O., Liu, D., Goetzl, E. J., Mattson, M. P., Greig, N. H., Eitan, E., & Kapogiannis, D. (2021). Neuronal and astrocytic extracellular vesicle biomarkers in blood reflect brain pathology in mouse models of Alzheimer's disease. *Cells*, 10(5), 993.
- DeMattos, R. B., O'dell, M. A., Parsadanian, M., Taylor, J. W., Harmony, J. A., Bales, K. R., Paul, S. M., Aronow, B. J., & Holtzman, D. M. (2002). Clusterin promotes amyloid plaque formation and is critical for neuritic toxicity in a mouse model of Alzheimer's disease. *Proceedings of the National Academy of Sciences of the United States of America*, 99(16), 10843–10848.
- Day, S. M., Gironda, S. C., Clarke, C. W., Snipes, J. A., Nicol, N. I., Kamran, H., Vaughn, W., Weiner, J. L., & Macauley, S. L. (2022). Ethanol exposure alters Alzheimer's-related pathology, behavior, and metabolism in APP/PS1 mice. *Neurobiology Disease*, 177, 105967. <https://doi.org/10.1016/j.nbd.2022.105967>
- Eitan, E., Green, J., Bodogai, M., Mode, N. A., Bæk, R., Jørgensen, M. M., Freeman, D. W., Witwer, K. W., Zonderman, A. B., Biragyn, A., Mattson, M. P., Noren Hooten, N., & Evans, M. K. (2017). Age-related changes in plasma extracellular vesicle characteristics and internalization by leukocytes. *Scientific Reports*, 7(1), 1342.
- Eren, E., Leoutsakos, J. M., Troncoso, J., Lyketos, C. G., Oh, E. S., & Kapogiannis, D. (2022). Neuronal-derived EV biomarkers track cognitive decline in Alzheimer's disease. *Cells*, 11(3), 436.
- Fagan, A. M., Mintun, M. A., Mach, R. H., Lee, S. Y., Dence, C. S., Shah, A. R., LaRossa, G. N., Spinner, M. L., Klunk, W. E., Mathis, C. A., DeKosky, S. T., Morris, J. C., & Holtzman, D. M. (2006). Inverse relation between in vivo amyloid imaging load and cerebrospinal fluid Abeta42 in humans. *Annals of Neurology*, 59(3), 512–519.
- Ferreira, P. G., Muñoz-Aguirre, M., Reverter, F., Sá Godinho, C. P., Sousa, A., Amadoz, A., Sodaei, R., Hidalgo, M. R., Pervouchine, D., Carbonell-Caballero, J., Nurdinov, R., Breschi, A., Amador, R., Oliveira, P., Çubuk, C., Curado, J., Aguet, F., Oliveira, C., Dopazo, J., ... Guigó, R. (2018). The effects of death and post-mortem cold ischemia on human tissue transcriptomes. *Nature Communications*, 9(1), 490.
- Gallagher, J. J., Minogue, A. M., & Lynch, M. A. (2013). Impaired performance of female APP/PS1 mice in the Morris water maze is coupled with increased A $\beta$  accumulation and microglial activation. *Neuro-Degenerative Diseases*, 11(1), 33–41.
- Gallart-Palau, X., Serra, A., Hase, Y., Tan, C. F., Chen, C. P., Kalara, R. N., & Sze, S. K. (2019). Brain-derived and circulating vesicle profiles indicate neurovascular unit dysfunction in early Alzheimer's disease. *Brain Pathology*, 29(5), 593–605.
- Gallart-Palau, X., Serra, A., & Sze, S. K. (2016). Enrichment of extracellular vesicles from tissues of the central nervous system by PROSPR. *Molecular Neurodegeneration*, 11(1), 41.
- Gauthier, S. A., Pérez-González, R., Sharma, A., Huang, F. K., Alldred, M. J., Pawlik, M., Kaur, G., Ginsberg, S. D., Neubert, T. A., & Levy, E. (2017). Enhanced exosome secretion in Down syndrome brain—a protective mechanism to alleviate neuronal endosomal abnormalities. *Acta Neuropathologica Communications*, 5(1), 65.
- Goetzl, E. J., Boxer, A., Schwartz, J. B., Abner, E. L., Petersen, R. C., Miller, B. L., & Kapogiannis, D. (2015). Altered lysosomal proteins in neural-derived plasma exosomes in preclinical Alzheimer disease. *Neurology*, 85(1), 40–47.
- Goetzl, E. J., Mustapic, M., Kapogiannis, D., Eitan, E., Lobach, I. V., Goetzl, L., Schwartz, J. B., & Miller, B. L. (2016). Cargo proteins of plasma astrocyte-derived exosomes in Alzheimer's disease. *FASEB Journal: Official Publication of the Federation of American Societies for Experimental Biology*, 30(11), 3853–3859.
- Grizzanti, J., Moritz, W. R., Pait, M. C., Stanley, M., Kaye, S. D., Carroll, C. M., Constantino, N. J., Deitelzweig, L. J., Snipes, J. A., Kellar, D., Caesar, E. E., Pettit-Mee, R. J., Day, S. M., Sens, J. P., Nicol, N. I., Dhillon, J., Remedi, M. S., Kiraly, D. D., Karch, C. M., ... Macauley, S. L. (2023). KATP channels are necessary for glucose-dependent increases in amyloid-beta and Alzheimer's disease-related pathology. *JCI Insight*, 8(10), e162454.
- Guillot-Sestier, M. V., Araiz, A. R., Mela, V., Gaban, A. S., O'Neill, E., Joshi, L., Chouchani, E. T., Mills, E. L., & Lynch, M. A. (2021). Microglial metabolism is a pivotal factor in sexual dimorphism in Alzheimer's disease. *Communications Biology*, 4(1), 711.
- Guo, M., Wang, J., Zhao, Y., Feng, Y., Han, S., Dong, Q., Cui, M., & Tieu, K. (2020). Microglial exosomes facilitate  $\alpha$ -synuclein transmission in Parkinson's disease. *Brain: A Journal of Neurology*, 143(5), 1476–1497.
- Harris, R. A., Tindale, L., Lone, A., Singh, O., Macauley, S. L., Stanley, M., Holtzman, D. M., Bartha, R., & Cumming, R. C. (2016). Aerobic glycolysis in the frontal cortex correlates with memory performance in wild-type mice but not the APP/PS1 mouse model of cerebral amyloidosis. *The Journal of Neuroscience: The Official Journal of the Society for Neuroscience*, 36(6), 1871–1878.
- Harrison, E. B., Hochfelder, C. G., Lamberty, B. G., Meays, B. M., Morsey, B. M., Kelso, M. L., Fox, H. S., & Yelamanchili, S. V. (2016). Traumatic brain injury increases levels of miR-21 in extracellular vesicles: Implications for neuroinflammation. *FEBS Open Bio*, 6(8), 835–846.
- Hartley, D., Blumenthal, T., Carrillo, M., DiPaolo, G., Esralew, L., Gardiner, K., Granholm, A. C., Iqbal, K., Krams, M., Lemere, C., Lott, I., Mobley, W., Ness, S., Nixon, R., Potter, H., Reeves, R., Sabbagh, M., Silverman, W., Tycko, B., ... Wisniewski, T. (2015). Down syndrome and Alzheimer's disease: Common pathways, common goals. *Alzheimer's & Dementia: the Journal of the Alzheimer's Association*, 11(6), 700–709.
- Hernández-Ortega, K., Garcia-Esparcia, P., Gil, L., Lucas, J. J., & Ferrer, I. (2016). Altered machinery of protein synthesis in Alzheimer's: From the nucleolus to the ribosome. *Brain Pathology*, 26(5), 593–605.
- Holth, J. K., Fritsch, S. K., Wang, C., Pedersen, N. P., Cirrito, J. R., Mahan, T. E., Finn, M. B., Manis, M., Geerling, J. C., Fuller, P. M., Lucey, B. P., & Holtzman, D. M. (2019). The sleep-wake cycle regulates brain interstitial fluid tau in mice and CSF tau in humans. *Science*, 363(6429), 880–884.
- Holtzman, D. M. (2004). In vivo effects of ApoE and clusterin on amyloid-beta metabolism and neuropathology. *Journal of Molecular Neuroscience: MN*, 23(3), 247–254.
- Holtzman, D. M., Morris, J. C., & Goate, A. M. (2011). Alzheimer's disease: The challenge of the second century. *Science Translational Medicine*, 3(77), 77sr1.
- Hong, S., Quintero-Monzon, O., Ostaszewski, B. L., Podlisny, D. R., Cavanaugh, W. T., Yang, T., Holtzman, D. M., Cirrito, J. R., & Selkoe, D. J. (2011). Dynamic analysis of amyloid beta-protein in behaving mice reveals opposing changes in ISF versus parenchymal A $\beta$  during age-related plaque formation. *The Journal of Neuroscience: The Official Journal of the Society for Neuroscience*, 31(44), 15861–15869.

- Huang, Y. (2022). Brain tissue-derived extracellular vesicles in Alzheimer's disease display altered key protein levels including cell type-specific markers. *Journal of Alzheimer's Disease*, 39(3), 1057–1072.
- Huang, Y., Cheng, L., Turchinovich, A., Mahairaki, V., Troncoso, J. C., Pletniková, O., Haughey, N. J., Vella, L. J., Hill, A. F., Zheng, L., & Witwer, K. W. (2020). Influence of species and processing parameters on recovery and content of brain tissue-derived extracellular vesicles. *Journal of Extracellular Vesicles*, 9(1), 1785746.
- Hurwitz, S. N., Sun, L., Cole, K. Y., Ford, C. R., 3rd, Olcese, J. M., & Meckes, D. G. Jr (2018). An optimized method for enrichment of whole brain-derived extracellular vesicles reveals insight into neurodegenerative processes in a mouse model of Alzheimer's disease. *Journal of Neuroscience Methods*, 307, 210–220.
- Iwatsubo, T., Odaka, A., Suzuki, N., Mizusawa, H., Nukina, N., & Ihara, Y. (1994). Visualization of A beta 42(43) and A beta 40 in senile plaques with end-specific A beta monoclonals: Evidence that an initially deposited species is A beta 42(43). *Neuron*, 13(1), 45–53.
- Jankowsky, J. L., Fadale, D. J., Anderson, J., Xu, G. M., Gonzales, V., Jenkins, N. A., Copeland, N. G., Lee, M. K., Younkin, L. H., Wagner, S. L., Younkin, S. G., & Borchelt, D. R. (2004). Mutant presenilins specifically elevate the levels of the 42 residue beta-amyloid peptide in vivo: Evidence for augmentation of a 42-specific gamma secretase. *Human Molecular Genetics*, 13(2), 159–170.
- Jarrett, J. T., Berger, E. P., & Lansbury, P. T. Jr (1993). The carboxy terminus of the beta amyloid protein is critical for the seeding of amyloid formation: Implications for the pathogenesis of Alzheimer's disease. *Biochemistry*, 32(18), 4693–4697.
- Jeppesen, D. K., Fenix, A. M., Franklin, J. L., Higginbotham, J. N., Zhang, Q., Zimmerman, L. J., Liebler, D. C., Ping, J., Liu, Q., Evans, R., Fissell, W. H., Patton, J. G., Rome, L. H., Burnette, D. T., & Coffey, R. J. (2019). Reassessment of exosome composition. *Cell*, 177(2), 428–445.e18.
- Jia, L., Qiu, Q., Zhang, H., Chu, L., Du, Y., Zhang, J., Zhou, C., Liang, F., Shi, S., Wang, S., Qin, W., Wang, Q., Li, F., Wang, Q., Li, Y., Shen, L., Wei, Y., & Jia, J. (2019). Concordance between the assessment of Aβ42, T-tau, and P-T181-tau in peripheral blood neuronal-derived exosomes and cerebrospinal fluid. *Alzheimer's & Dementia: The Journal of the Alzheimer's Association*, 15(8), 1071–1080.
- Juras, J. A., Webb, M. B., Young, L. E. A., Markussen, K. H., Hawkinson, T. R., Buoncristiani, M. D., Bolton, K. E., Coburn, P. T., Williams, M. I., Sun, L. P. Y., Sanders, W. C., Bruntz, R. C., Conroy, L. R., Wang, C., Gentry, M. S., Smith, B. N., & Sun, R. C. (2023). In situ microwave fixation provides an instantaneous snapshot of the brain metabolome. *Cell Rep Methods*, 3(4), 100455. <https://doi.org/10.1016/j.crmeth.2023.100455>
- Kakarla, R., Hur, J., Kim, Y. J., Kim, J., & Chwae, Y. J. (2020). Apoptotic cell-derived exosomes: Messages from dying cells. *Experimental & Molecular Medicine*, 52(1), 1–6.
- Kamenetz, F., Tomita, T., Hsieh, H., Seabrook, G., Borchelt, D., Iwatsubo, T., Sisodia, S., & Malinow, R. (2003). APP processing and synaptic function. *Neuron*, 37(6), 925–937.
- Kang, J. E., Lim, M. M., Bateman, R. J., Lee, J. J., Smyth, L. P., Cirrito, J. R., Fujiki, N., Nishino, S., & Holtzman, D. M. (2009). Amyloid-beta dynamics are regulated by orexin and the sleep-wake cycle. *Science*, 326(5955), 1005–1007.
- Kapogiannis, D., Boxer, A., Schwartz, J. B., Abner, E. L., Biragyn, A., Masharani, U., Frassetto, L., Petersen, R. C., Miller, B. L., & Goetzl, E. J. (2015). Dysfunctionally phosphorylated type 1 insulin receptor substrate in neural-derived blood exosomes of preclinical Alzheimer's disease. *FASEB Journal: Official Publication of the Federation of American Societies for Experimental Biology*, 29(2), 589–596.
- Kaushik, S., & Cuervo, A. M. (2015). Proteostasis and aging. *Nature Medicine*, 21(12), 1406–1415.
- Keerthikumar, S., Chisanga, D., Ariyaratne, D., Al Saffar, H., Anand, S., Zhao, K., Samuel, M., Pathan, M., Jois, M., Chilamkurti, N., Gangoda, L., & Mathivanan, S. (2016). ExoCarta: A web-based compendium of exosomal cargo. *Journal of Molecular Biology*, 428(4), 688–692.
- Koga, H., Kaushik, S., & Cuervo, A. M. (2011). Protein homeostasis and aging: The importance of exquisite quality control. *Ageing Research Reviews*, 10(2), 205–215.
- Kolter, T., & Sandhoff, K. (2005). Principles of lysosomal membrane digestion: Stimulation of sphingolipid degradation by sphingolipid activator proteins and anionic lysosomal lipids. *Annual Review of Cell and Developmental Biology*, 21, 81–103.
- Kumar, A., Kim, S., Su, Y., Sharma, M., Kumar, P., Singh, S., Lee, J., Furdul, C. M., Singh, R., Hsu, F. C., Kim, J., Whitlow, C. T., Nader, M. A., & Deep, G. (2021). Brain cell-derived exosomes in plasma serve as neurodegeneration biomarkers in male cynomolgus monkeys self-administering oxycodone. *EBioMedicine*, 63, 103192.
- Kumar, A., Sharma, M., Su, Y., Singh, S., Hsu, F. C., Neth, B. J., Register, T. C., Blennow, K., Zetterberg, H., Craft, S., & Deep, G. (2022). Small extracellular vesicles in plasma reveal molecular effects of modified Mediterranean-ketogenic diet in participants with mild cognitive impairment. *Brain Communications*, 4(6), fca262.
- Kumar, A., Su, Y., Sharma, M., Singh, S., Kim, S., Peavey, J. J., Suerken, C. K., Lockhart, S. N., Whitlow, C. T., Craft, S., Hughes, T. M., & Deep, G. (2023). MicroRNA expression in extracellular vesicles as a novel blood-based biomarker for Alzheimer's disease. *Alzheimer's & Dementia: The Journal of the Alzheimer's Association*, 19(11), 4952–4966.
- Lazo, S., Noren Hooten, N., Green, J., Eitan, E., Mode, N. A., Liu, Q. R., Zonderman, A. B., Ezike, N., Mattson, M. P., Ghosh, P., & Evans, M. K. (2021). Mitochondrial DNA in extracellular vesicles declines with age. *Ageing Cell*, 20(1), e13283.
- Lee, J. H., Ostalecki, C., Oberstein, T., Schierer, S., Zinser, E., Eberhardt, M., Blume, K., Plosnita, B., Stich, L., Bruns, H., Coras, R., Vera-Gonzales, J., Maler, M., & Baur, A. S. (2022). Alzheimer's disease protease-containing plasma extracellular vesicles transfer to the hippocampus via the choroid plexus. *EBioMedicine*, 77, 103903.
- Lim, C. Z. J., Zhang, Y., Chen, Y., Zhao, H., Stephenson, M. C., Ho, N. R. Y., Chen, Y., Chung, J., Reilhac, A., Loh, T. P., Chen, C. L. H., & Shao, H. (2019). Subtyping of circulating exosome-bound amyloid β reflects brain plaque deposition. *Nature Communications*, 10(1), 1144.
- Longobardi, A., Benussi, L., Nicsanu, R., Bellini, S., Ferrari, C., Saraceno, C., Zanardini, R., Catania, M., Di Fede, G., Squitti, R., Binetti, G., & Ghidoni, R. (2021). Plasma extracellular vesicle size and concentration are altered in Alzheimer's disease, dementia with lewy bodies, and frontotemporal dementia. *Frontiers in Cell and Developmental Biology*, 9, 667369.
- Longobardi, A., Nicsanu, R., Bellini, S., Squitti, R., Catania, M., Tiraboschi, P., Saraceno, C., Ferrari, C., Zanardini, R., Binetti, G., Di Fede, G., Benussi, L., & Ghidoni, R. (2022). Cerebrospinal fluid EV concentration and size are altered in Alzheimer's disease and dementia with lewy bodies. *Cells*, 11(3), 462.
- Lynch, M. A. (2022). Exploring Sex-related differences in microglia may be a game-changer in precision medicine. *Frontiers in Aging Neuroscience*, 14, 868448.
- Macauley, S. L., Stanley, M., Caesar, E. E., Yamada, S. A., Raichle, M. E., Perez, R., Mahan, T. E., Sutphen, C. L., & Holtzman, D. M. (2015). Hyperglycemia modulates extracellular amyloid-β concentrations and neuronal activity in vivo. *The Journal of Clinical Investigation*, 125(6), 2463–2467.
- Macauley, S. L., Stanley, M. S., Caesar, E. E., Moritz, W. R., Bice, A. R., Cruz-Diaz, N., Carroll, C. M., Day, S. M., Grizzanti, J., Mahan, T. E., Snipes, J. A., Orr, T. E., Culver, J. P., Remedi, M. S., Nichols, C. G., Karch, C. M., Cox, L. A., Diz, D. I., Bauer, A. Q., & Holtzman, D. M. (2021). Sulfonyleureas target the neurovascular response to decrease Alzheimer's pathology. *bioRxiv*, <https://doi.org/10.1101/2021.08.11.455969>
- Manocha, G. D., Floden, A. M., Rausch, K., Kulas, J. A., McGregor, B. A., Rojanathammanee, L., Puig, K. R., Puig, K. L., Karki, S., Nichols, M. R., Darland, D. C., Porter, J. E., & Combs, C. K. (2016). APP regulates microglial phenotype in a mouse model of Alzheimer's disease. *The Journal of Neuroscience: The Official Journal of the Society for Neuroscience*, 36(32), 8471–8486.



- Mathews, P. M., & Levy, E. (2019). Exosome production is key to neuronal endosomal pathway integrity in neurodegenerative diseases. *Frontiers in Neuroscience*, 13, 1347.
- Meng, X., Yang, S., & Camp, V. J. A. (2020). The interplay between the DNA damage response, RNA processing and extracellular vesicles. *Frontiers in Oncology*, 9, 1538.
- Mishra, S., Kumar, A., Kim, S., Su, Y., Singh, S., Sharma, M., Almousa, S., Rather, H. A., Jain, H., Lee, J., Furdui, C. M., Ahmad, S., Ferrario, C. M., Punzi, H. A., Chuang, C. C., Wabitsch, M., Kritchevsky, S. B., Register, T. C., & Deep, G. (2023). A liquid biopsy-based approach to isolate and characterize adipose tissue-derived extracellular vesicles from blood. *ACS Nano*, 17(11), 10252–10268.
- Muraoka, S., DeLeo, A. M., Sethi, M. K., Yukawa-Takamatsu, K., Yang, Z., Ko, J., Hogan, J. D., Ruan, Z., You, Y., Wang, Y., Medalla, M., Ikezu, S., Chen, M., Xia, W., Gorantla, S., Gendelman, H. E., Issadore, D., Zaia, J., & Ikezu, T. (2020). Proteomic and biological profiling of extracellular vesicles from Alzheimer's disease human brain tissues. *Alzheimer's & Dementia: The Journal of the Alzheimer's Association*, 16(6), 896–907.
- Muraoka, S., Jedrychowski, M. P., Iwahara, N., Abdullah, M., Onos, K. D., Keezer, K. J., Hu, J., Ikezu, S., Howell, G. R., Gygi, S. P., & Ikezu, T. (2021). Enrichment of neurodegenerative microglia signature in brain-derived extracellular vesicles isolated from Alzheimer's disease mouse models. *Journal of Proteome Research*, 20(3), 1733–1743.
- Muraoka, S., Jedrychowski, M. P., Yanamandra, K., Ikezu, S., Gygi, S. P., & Ikezu, T. (2020). Proteomic profiling of extracellular vesicles derived from cerebrospinal fluid of Alzheimer's disease patients: A pilot study. *Cells*, 9(9), 1959.
- Muraoka, S., Lin, W., Chen, M., Hersch, S. W., Emili, A., Xia, W., & Ikezu, T. (2020). Assessment of separation methods for extracellular vesicles from human and mouse brain tissues and human cerebrospinal fluids. *Methods*, 177, 35–49.
- Ngolab, J., Trinh, I., Rockenstein, E., Mante, M., Florio, J., Trejo, M., Masliah, D., Adame, A., Masliah, E., & Rissman, R. A. (2017). Brain-derived exosomes from dementia with Lewy bodies propagate  $\alpha$ -synuclein pathology. *Acta Neuropathologica Communications*, 5(1), 46.
- Nguyen, N. P., Helmbrecht, H., Ye, Z., Adebayo, T., Hashi, N., Doan, M. A., & Nance, E. (2022). Brain tissue-derived extracellular vesicle mediated therapy in the neonatal ischemic brain. *International Journal of Molecular Sciences*, 23(2), 620.
- O'Brien, K., Breyne, K., Ughetto, S., Laurent, L. C., & Breakefield, X. O. (2020). RNA delivery by extracellular vesicles in mammalian cells and its applications. *Nature Reviews. Molecular Cell Biology*, 21(10), 585–606.
- Oggero, S., Austin-Williams, S., & Norling, L. V. (2019). The contrasting role of extracellular vesicles in vascular inflammation and tissue repair. *Frontiers in Pharmacology*, 10, 1479.
- Peng, K. Y., Pérez-González, R., Alldred, M. J., Goulbourne, C. N., Morales-Corraliza, J., Saito, M., Saito, M., Ginsberg, S. D., Mathews, P. M., & Levy, E. (2019). Apolipoprotein E4 genotype compromises brain exosome production. *Brain: A Journal of Neurology*, 142(1), 163–175.
- Perez-Gonzalez, R., Gauthier, S. A., Kumar, A., & Levy, E. (2012). The exosome secretory pathway transports amyloid precursor protein carboxyl-terminal fragments from the cell into the brain extracellular space. *The Journal of Biological Chemistry*, 287(51), 43108–43115.
- Pérez-González, R., Gauthier, S. A., Kumar, A., Saito, M., Saito, M., & Levy, E. (2017). A method for isolation of extracellular vesicles and characterization of exosomes from brain extracellular space. *Methods in Molecular Biology*, 1545, 139–151.
- Polanco, J. C., Scicluna, B. J., Hill, A. F., & Götz, J. (2016). Extracellular vesicles isolated from the brains of rTg4510 mice seed tau protein aggregation in a threshold-dependent manner. *The Journal of Biological Chemistry*, 291(24), 12445–12466.
- Powers, E. T., Morimoto, R. I., Dillin, A., Kelly, J. W., & Balch, W. E. (2009). Biological and chemical approaches to diseases of proteostasis deficiency. *Annual Review of Biochemistry*, 78, 959–991.
- Rajendran, L., Honsho, M., Zahn, T. R., Keller, P., Geiger, K. D., Verkade, P., & Simons, K. (2006). Alzheimer's disease beta-amyloid peptides are released in association with exosomes. *Proceedings of the National Academy of Sciences of the United States of America*, 103(30), 11172–11177.
- Rather, H. A., Mishra, S., Su, Y., Kumar, A., Singh, S., Misra, B. B., Lee, J., Furdui, C. M., Hamilton, L. R., Gould, R. W., Nader, S. H., Nader, M. A., & Deep, G. (2022). Mass spectrometry-based proteome profiling of extracellular vesicles derived from the cerebrospinal fluid of adult rhesus monkeys exposed to cocaine throughout gestation. *Biomolecules*, 12(4), 510.
- Roh, J. H., Huang, Y., Bero, A. W., Kasten, T., Stewart, F. R., Bateman, R. J., & Holtzman, D. M. (2012). Disruption of the sleep-wake cycle and diurnal fluctuation of  $\beta$ -amyloid in mice with Alzheimer's disease pathology. *Science Translational Medicine*, 4(150), 150ra122.
- Ruan, Z., Delpech, J. C., Venkatesan Kalavai, S., Van Enoo, A. A., Hu, J., Ikezu, S., & Ikezu, T. (2020). P2RX7 inhibitor suppresses exosome secretion and disease phenotype in P301S tau transgenic mice. *Molecular Neurodegeneration*, 15(1), 47.
- Ruan, Z., Pathak, D., Venkatesan Kalavai, S., Yoshii-Kitahara, A., Muraoka, S., Bhatt, N., Takamatsu-Yukawa, K., Hu, J., Wang, Y., Hersch, S., Ericsson, M., Gorantla, S., Gendelman, H. E., Kaye, R., Ikezu, S., Luebke, J. I., & Ikezu, T. (2020). Alzheimer's disease brain-derived extracellular vesicles spread tau pathology in interneurons. *Brain*, 144(1), 288–309.
- Sala Frigerio, C., Wolfs, L., Fattorelli, N., Thrupp, N., Voytyuk, I., Schmidt, I., Mancuso, R., Chen, W. T., Woodbury, M. E., Srivastava, G., Möller, T., Hudry, E., Das, S., Saido, T., Karran, E., Hyman, B., Perry, V. H., Fiers, M., & De Strooper, B. (2019). The Major risk factors for Alzheimer's disease: Age, sex, and genes modulate the microglia response to A $\beta$  plaques. *Cell Reports*, 27(4), 1293–1306.e6.
- Sardar Sinha, M., Ansell-Schultz, A., Civitelli, L., Hildesjö, C., Larsson, M., Lannfelt, L., Ingelsson, M., & Hallbeck, M. (2018). Alzheimer's disease pathology propagation by exosomes containing toxic amyloid-beta oligomers. *Acta Neuropathologica*, 136(1), 41–56.
- Schindler, S. E., Gray, J. D., Gordon, B. A., Xiong, C., Batrla-Utermann, R., Quan, M., Wahl, S., Benzinger, T. L. S., Holtzman, D. M., Morris, J. C., & Fagan, A. M. (2018). Cerebrospinal fluid biomarkers measured by Elecsys assays compared to amyloid imaging. *Alzheimer's & Dementia: The journal of the Alzheimer's Association*, 14(11), 1460–1469.
- Shippy, D. C., & Ulland, T. K. (2020). Microglial immunometabolism in Alzheimer's disease. *Frontiers in Cellular Neuroscience*, 14, 563446.
- Skotland, T., Sagini, K., Sandvig, K., & Llorente, A. (2020). An emerging focus on lipids in extracellular vesicles. *Advanced Drug Delivery Reviews*, 159, 308–321.
- Spitzer, P., Mulzer, L. M., Oberstein, T. J., Munoz, L. E., Lewczuk, P., Kornhuber, J., Herrmann, M., & Maler, J. M. (2019). Microvesicles from cerebrospinal fluid of patients with Alzheimer's disease display reduced concentrations of tau and APP protein. *Scientific Reports*, 9(1), 7089.
- Stanley, M., Macauley, S. L., Caesar, E. E., Koscal, L. J., Moritz, W., Robinson, G. O., Roh, J., Keyser, J., Jiang, H., & Holtzman, D. M. (2016). The effects of peripheral and central high insulin on brain insulin signaling and amyloid-beta in young and old APP/PS1 mice. *The Journal of Neuroscience: The Official Journal of the Society for Neuroscience*, 36(46), 11704–11715.
- Stauffer, W., Sheng, H., & Lim, H. N. (2018). EzColocalization: An ImageJ plugin for visualizing and measuring colocalization in cells and organisms. *Scientific Reports*, 8(1), 15764.
- Su, H., Rustam, Y. H., Masters, C. L., Makalic, E., McLean, C. A., Hill, A. F., Barnham, K. J., Reid, G. E., & Vella, L. J. (2021). Characterization of brain-derived extracellular vesicle lipids in Alzheimer's disease. *Journal of Extracellular Vesicles*, 10(7), e12089.

- Szklarczyk, D., Kirsch, R., Koutrouli, M., Nastou, K., Mehryary, F., Hachilif, R., Gable, A. L., Fang, T., Doncheva, N. T., Pyysalo, S., Bork, P., Jensen, L. J., & von Mering, C. (2023). The STRING database in 2023: Protein-protein association networks and functional enrichment analyses for any sequenced genome of interest. *Nucleic Acids Research*, 51(D1), D638–D646.
- Takahashi, H., Klein, Z. A., Bhagat, S. M., Kaufman, A. C., Kostylev, M. A., Ikezu, T., Strittmatter, S. M., & Alzheimer's Disease Neuroimaging Initiative. (2017). Opposing effects of progranulin deficiency on amyloid and tau pathologies via microglial TYROBP network. *Acta Neuropathologica*, 133(5), 785–807.
- Théry, C., Witwer, K. W., Aikawa, E., Alcaraz, M. J., Anderson, J. D., Andriantsitohaina, R., Antoniou, A., Arab, T., Archer, F., Atkin-Smith, G. K., Ayre, D. C., Bach, J. M., Bachurski, D., Baharvand, H., Balaj, L., Baldacchino, S., Bauer, N. N., Baxter, A. A., Bebawy, M., ... Zuba-Surma, E. K. (2018). Minimal information for studies of extracellular vesicles 2018 (MISEV2018): A position statement of the International Society for Extracellular Vesicles and update of the MISEV2014 guidelines. *Journal of Extracellular Vesicles*, 7(1), 1535750.
- Ulrich, J. D., Burchett, J. M., Restivo, J. L., Schuler, D. R., Verghese, P. B., Mahan, T. E., Landreth, G. E., Castellano, J. M., Jiang, H., Cirrito, J. R., & Holtzman, D. M. (2013). In vivo measurement of apolipoprotein E from the brain interstitial fluid using microdialysis. *Molecular Neurodegeneration*, 8, 13.
- UniProt Consortium. (2021). UniProt: The universal protein knowledgebase in 2021. *Nucleic Acids Research*, 49(D1), D480–D489.
- Utz, J., Berner, J., Muñoz, L. E., Oberstein, T. J., Kornhuber, J., Herrmann, M., Maler, J. M., & Spitzer, P. (2021). Cerebrospinal Fluid of patients with Alzheimer's disease contains increased percentages of synaptophysin-bearing microvesicles. *Frontiers in Aging Neuroscience*, 13, 682115.
- Vandendriessche, C., Balusu, S., Van Cauwenberghe, C., Brkic, M., Pauwels, M., Plehiers, N., Bruggeman, A., Dujardin, P., Van Imschoot, G., Van Wonterghem, E., Hendrix, A., Baeke, F., De Rycke, R., Gevaert, K., & Vandenbroucke, R. E. (2021). Importance of extracellular vesicle secretion at the blood-cerebrospinal fluid interface in the pathogenesis of Alzheimer's disease. *Acta Neuropathologica Communications*, 9(1), 143.
- van Niel, G., D'Angelo, G., & Raposo, G. (2018). Shedding light on the cell biology of extracellular vesicles. *Nature Reviews. Molecular cell biology*, 19(4), 213–228.
- Vassileff, N., Vella, L. J., Rajapaksha, H., Shambrook, M., Kenari, A. N., McLean, C., Hill, A. F., & Cheng, L. (2020). Revealing the proteome of motor cortex derived extracellular vesicles isolated from amyotrophic lateral sclerosis human postmortem tissues. *Cells*, 9(7), 1709.
- Vella, L. J., Scicluna, B. J., Cheng, L., Bawden, E. G., Masters, C. L., Ang, C. S., Williamson, N., McLean, C., Barnham, K. J., & Hill, A. F. (2017). A rigorous method to enrich for exosomes from brain tissue. *Journal of Extracellular Vesicles*, 6(1), 1348885.
- Wang, Y., Balaji, V., Kaniyappan, S., Krüger, L., Irsen, S., Tepper, K., Chandupatla, R., Maetzler, W., Schneider, A., Mandelkow, E., & Mandelkow, E. M. (2017). The release and trans-synaptic transmission of Tau via exosomes. *Molecular Neurodegeneration*, 12(1), 5.
- Wei, F., Wang, A., Wang, Q., Han, W., Rong, R., Wang, L., Liu, S., Zhang, Y., Dong, C., & Li, Y. (2020). Plasma endothelial cells-derived extracellular vesicles promote wound healing in diabetes through YAP and the PI3K/Akt/mTOR pathway. *Aging*, 12(12), 12002–12018.
- Winston, C. N., Aulston, B., Rockenstein, E. M., Adame, A., Prikhodko, O., Dave, K. N., Mishra, P., Rissman, R. A., & Yuan, S. H. (2019). Neuronal Exosome-Derived Human Tau is Toxic to Recipient Mouse Neurons in vivo. *Journal of Alzheimer's Disease: JAD*, 67(2), 541–553.
- Winston, C. N., Goetzl, E. J., Akers, J. C., Carter, B. S., Rockenstein, E. M., Galasko, D., Masliah, E., & Rissman, R. A. (2016). Prediction of conversion from mild cognitive impairment to dementia with neuronally derived blood exosome protein profile. *Alzheimer's & Dementia (Amsterdam)*, 3, 63–72.
- Winston, C. N., Goetzl, E. J., Schwartz, J. B., Elahi, F. M., & Rissman, R. A. (2019). Complement protein levels in plasma astrocyte-derived exosomes are abnormal in conversion from mild cognitive impairment to Alzheimer's disease dementia. *Alzheimer's & Dementia (Amsterdam)*, 11, 61–66.
- Wisniewski, K. E., Wisniewski, H. M., & Wen, G. Y. (1985). Occurrence of neuropathological changes and dementia of Alzheimer's disease in Down's syndrome. *Annals of Neurology*, 17(3), 278–282.
- Yamada, K. (2018). In vivo microdialysis method to collect large extracellular proteins from brain interstitial fluid with high-molecular weight cut-off probes. *Journal of Visualized Experiments: JoVE*, 2018(139), 57869. <https://doi.org/10.3791/57869>
- Yamada, K., Cirrito, J. R., Stewart, F. R., Jiang, H., Finn, M. B., Holmes, B. B., Binder, L. I., Mandelkow, E. M., Diamond, M. I., Lee, V. M., & Holtzman, D. M. (2011). In vivo microdialysis reveals age-dependent decrease of brain interstitial fluid tau levels in P301S human tau transgenic mice. *The Journal of Neuroscience: The Official Journal of the Society for Neuroscience*, 31(37), 13110–13117.
- Yamada, K., Holth, J. K., Liao, F., Stewart, F. R., Mahan, T. E., Jiang, H., Cirrito, J. R., Patel, T. K., Hochgräfe, K., Mandelkow, E. M., & Holtzman, D. M. (2014). Neuronal activity regulates extracellular tau in vivo. *The Journal of Experimental Medicine*, 211(3), 387–393.
- Yelamanchili, S. V., Lamberty, B. G., Rennard, D. A., Morsey, B. M., Hochfelder, C. G., Meays, B. M., Levy, E., & Fox, H. S. (2015). MiR-21 in extracellular vesicles leads to neurotoxicity via TLR7 signaling in SIV neurological disease. *PLoS Pathogens*, 11(7), e1005032.
- Yeung, C. C., Dondelinger, F., Schoof, E. M., Georg, B., Lu, Y., Zheng, Z., Zhang, J., Hannibal, J., Fahrenkrug, J., & Kjaer, M. (2022). Circadian regulation of protein cargo in extracellular vesicles. *Science Advances*, 8(14), eabc9061.
- Yuyama, K., Sun, H., Mitsutake, S., & Igarashi, Y. (2012). Sphingolipid-modulated exosome secretion promotes clearance of amyloid- $\beta$  by microglia. *The Journal of Biological Chemistry*, 287(14), 10977–10989.
- Yuyama, K., Sun, H., Usuki, S., Sakai, S., Hanamatsu, H., Mioka, T., Kimura, N., Okada, M., Tahara, H., Furukawa, J., Fujitani, N., Shinohara, Y., & Igarashi, Y. (2015). A potential function for neuronal exosomes: Sequestering intracerebral amyloid- $\beta$  peptide. *FEBS letters*, 589(1), 84–88.
- Zhang, Y., Chen, K., Sloan, S. A., Bennett, M. L., Scholze, A. R., O'Keeffe, S., Phatnani, H. P., Guarnieri, P., Caneda, C., Ruderisch, N., Deng, S., Liddelow, S. A., Zhang, C., Daneman, R., Maniatis, T., Barres, B. A., & Wu, J. Q. (2014). An RNA-sequencing transcriptome and splicing database of glia, neurons, and vascular cells of the cerebral cortex. *The Journal of Neuroscience: The Official Journal of the Society for Neuroscience*, 34(36), 11929–11947.

## SUPPORTING INFORMATION

Additional supporting information can be found online in the Supporting Information section at the end of this article.

**How to cite this article:** Pait, M. C., Kaye, S. D., Su, Y., Kumar, A., Singh, S., Gironda, S. C., Vincent, S., Anwar, M., Carroll, C. M., Snipes, J. A., Lee, J., Furdul, C. M., Deep, G., & Macauley, S. L. (2024). Novel method for collecting hippocampal interstitial fluid extracellular vesicles (EV<sup>ISF</sup>) reveals sex-dependent changes in microglial EV proteome in response to A $\beta$  pathology. *Journal of Extracellular Vesicles*, 13, e12398. <https://doi.org/10.1002/jev2.12398>